

High Precision Stabilization of Pan-Tilt Systems Using Reliable Angular Acceleration Feedback from a Master-Slave Kalman Filter

Sanem Evren · Fırat Yavuz · Mustafa Ünel

Received: 29 June 2016 / Accepted: 15 February 2017
© Springer Science+Business Media Dordrecht 2017

Abstract Pan-tilt robotic platforms are widely used to point sensor arrays (e.g. cameras, radars and antennas) in certain directions toward the target. Such platforms may suffer from external disturbances due to terrain changes, high-frequency vibrations and sudden shocks, wind and other environmental factors. These disturbances and hence small angular displacements may cause large position errors if the target is too far away. Therefore, high precision stabilization is required for these platforms to converge to the desired orientation and maintain it by rejecting unknown disturbances. In motion control, robust stabilization problem is usually tackled by employing angular acceleration feedback. However, obtaining reliable acceleration information is a challenging task. In this paper, we propose a novel master-slave type Kalman filter algorithm which consists of an extended Kalman filter (EKF) and an inverse Φ -algorithm in a master-slave configuration to estimate reliable angular acceleration signals by fusing 3-axis gyroscope, 3-axis accelerometer and 3-axis magnetometer data. Performance of the proposed sensor fusion algorithm

is evaluated on a high fidelity simulation model by using the estimated accelerations as feedback signals in the stabilization control of a 2-DOF pan-tilt system subject to external disturbances. As the acceleration feedback is incorporated into the control loop, higher stabilization is achieved. The performance of the proposed fusion algorithm is compared to Newton predictor enhanced Kalman filter (NPEKF) and the error state Kalman filter (ErKF). The proposed master-slave Kalman filter outperforms the Newton predictor enhanced Kalman filter whereas the results obtained by the proposed algorithm and the error state Kalman filter are comparable.

Keywords Angular acceleration · Sensor fusion · Extended Kalman filter · Inverse Φ -algorithm · Stabilization · Pan-tilt · Acceleration control

1 Introduction

Reliable position and orientation information is essential in the control of robotic platforms. Traditionally, joint angles are sensed by high resolution encoders or resolvers. In recent years, advances in the development of micro-electromechanical systems (MEMS) have significantly improved the cost-performance ratio of inertial sensors such as gyroscopes, accelerometers and magnetometers that measure angular velocities, linear accelerations and earth's magnetic field, respectively. These inertial sensor

S. Evren · F. Yavuz · M. Ünel (✉)
Faculty of Engineering and Natural Sciences, Sabancı
University, Istanbul, Turkey
e-mail: munel@sabanciuniv.edu

S. Evren
e-mail: sanemevren@sabanciuniv.edu

F. Yavuz
e-mail: firatyavuz@sabanciuniv.edu

measurements are used to determine attitude of rigid bodies in many applications such as unmanned vehicle control, platform stabilization, human motion tracking and underwater navigation [1–3]. The individual use of these sensors is not sufficient to determine attitude angles. For example, gyroscopes have high bandwidth and thus operate in a fast manner. However, they suffer from drift problems due to integration of gyro biases. On the other hand, accelerometers have low bandwidth and therefore they provide relatively accurate roll and pitch angles from the components of the gravity vector in a slow manner. Similarly, determining yaw angle from the components of the earth's magnetic field using a magnetometer is a drift-free but slow process. To obtain fast and accurate attitude angles, outputs of inertial sensors must be fused, i.e. sensor/data fusion.

Today, modern attitude and heading reference systems (AHRS) consist of an inertial measurement unit (IMU) and an onboard processor. A typical IMU is formed by a 3-axis gyroscope, a 3-axis accelerometer and a 3-axis magnetometer. A sensor fusion algorithm is employed in AHRS to combine individual sensor measurements to obtain more reliable attitude estimates. Sensor fusion algorithms eliminate disadvantages of inertial sensors and provide a complementary behavior where estimates mimic gyroscope measurements in the short term and accelerometer outputs in the long term.

Kalman filter [4] and its variations such as extended Kalman filter (EKF) [5, 6], unscented Kalman filter (UKF) [7] and adaptive Kalman filter (AKF) [8] are most widely used sensor fusion algorithms. Alternatively, an indirect Kalman filter approach (error state Kalman filter) has emerged to estimate the error in the state vector rather than the state itself [9, 10]. Due to the convergence problems in Kalman filtering, some researchers focused on the design and analysis of nonlinear observers to have good estimates from low cost inertial sensors [11–13]. Mahony et al. [11] proposed three nonlinear observers posed directly on the special orthogonal group ($\text{SO}(3)$) driven by reconstructed attitude and angular velocity measurements. Because of the similarity of the architecture to those of linear complementary filters, proposed observers are termed as direct complementary filter, passive complementary filter and explicit complementary filter. Both direct and passive filters can be

extended to estimate gyro biases online. The performance of the observers are demonstrated with a set of experiments performed on a robotic test bed and a radio controlled unmanned aerial vehicle. Bachman et al. [12] presented a quaternion-based complementary filter algorithm for processing the output data from nine-axis MARG (Magnetic field, Angular Rate, and Gravity) sensor unit containing three orthogonally mounted angular rate sensors, three orthogonal linear accelerometers and three orthogonal magnetometers. Madgwick [13] introduced a new orientation estimation algorithm that is applicable to both IMU and MARG systems. The algorithm employs a quaternion based representation of orientation to describe the coupled nature of orientations in three-dimensions and is not subject to the problematic singularities associated with an Euler angle representation.

Pan-tilt platforms are used to point sensor arrays (e.g. cameras, radars and antennas) in desired directions for different application areas such as target identification, security and defense, gun-turret control, search and rescue, entertainment and environmental monitoring [14–17]. These platforms are exposed to external disturbances due to terrain changes, high-frequency vibrations and sudden shocks, wind and other environmental factors. Therefore, unknown disturbances and even small angular displacements may cause large position errors if the target is too far away.

The goal of the stabilization control is to maintain the desired orientation by rejecting external disturbances. Since the effects of external disturbances can manifest themselves in the acceleration signals first, acceleration feedback can be utilized in high precision stabilization of robotic platforms. Schmidt and Lorenz [18] have showed that acceleration feedback acts as an electronic inertia to provide higher stiffness to the platform. Acceleration signals are incorporated as feedback into the following control techniques: the inner acceleration control [19], disturbance observer based control [3, 20], fuzzy control [21], feedforward compensation [22], adaptive inverse dynamic control [23] and contact transition control [24].

In spite of its great advantage in acceleration control, obtaining reliable acceleration feedback is quite challenging. Differentiation of measured position and velocity signals is not feasible due to sensor noise amplification problems. Angular accelerations can be measured by angular accelerometers which are costly and produced by few manufacturers. Therefore,

it is important to develop efficient angular acceleration estimation techniques. Several methods have been proposed in the literature. Han et al. [25] proposed a Newton Predictor Enhanced Kalman Filter (NPEKF) to estimate angular accelerations. This estimator provides a wide bandwidth and a small phase lag of the estimated acceleration while attenuating noises. Gyro free IMUs (GF-IMU) [26–28] that only use linear accelerometer measurements have been developed to estimate angular velocities and accelerations. Chen [26] presented a novel design of six-accelerometer configuration to compute the rotational and translational acceleration of a rigid body. The six-accelerometer design is in a cube structure; however, the computed angular velocity is derived by integrating the angular acceleration determined by accelerometer output. Due to the accumulated sensor biases in linear accelerometers, angular velocity error increases with time. Edwan et al. [27] presented an EKF based solution for the estimation of angular motion using a similar GF-IMU. The angular motion vector is determined by using 12 separate mono-axial linear accelerometers. This vector consists of angular accelerations and quadratic terms that include angular velocities. An EKF is used to estimate angular velocities and accelerations using this motion vector as measurements. The authors [28] also perform an observability analysis to determine the conditions for having an observable state vector.

In this paper, a new sensor fusion method for reliable angular acceleration estimation using a master-slave Kalman filter is presented. The proposed filter estimates the angular acceleration by extending the state vector of the AHRS problem to include both Euler rates and accelerations in addition to Euler angles and gyro biases. It employs both an extended Kalman filter (EKF) and an inverse Φ -algorithm in a master-slave configuration. While the master estimator (EKF) feeds the slave estimator (inverse Φ) with the estimated gyro biases, the slave estimates bias compensated angular velocity, acceleration and jerk signals in the body frame and sends back to the master. The proposed Kalman filter is developed in a master-slave configuration due to the following reasons:

- The master filter estimates the augmented state vector which includes gyro biases as well.

- The process dynamics of the new estimation problem needs the computation of body frame angular accelerations and jerks so a slave filter is required to estimate these accelerations and jerks and sends back to the master.
- The process dynamics of the new estimation problem requires the use of smooth and unbiased angular velocities to provide reliable Euler angle, velocity and acceleration information so a slave filter that utilizes the unbiased gyroscope measurements is developed to obtain smooth and unbiased estimates of angular velocities and sends back to the master.
- In the slave filter, unbiased gyroscope velocities are used as where the bias estimated by the master filter is subtracted from the gyroscope measurement.

The master-slave filter is used to obtain reliable estimates which are required to be used as feedback signals in the stabilization control of a 2-DOF pan-tilt platform. The performance of the stabilization control largely depends on the reliable feedback information. When the pan-tilt platform is subject to external disturbances, especially the use of reliable acceleration feedback improves the robustness of the system against the disturbances. Results obtained from a high fidelity simulation model which consists of the nonlinear dynamical model of the pan-tilt system subject to external disturbances and models of the inertial sensors (gyroscopes, accelerometers and magnetometers), demonstrate better performance of the PI controller enhanced with acceleration feedback over the conventional PI controller which does not utilize such feedback. As a result, the followings are the contributions of this work:

- A new estimation problem is stated by extending the state vector of AHRS to include both Euler rates and accelerations in addition to Euler angles and gyro biases. Thus, the state dimension of AHRS problem is increased from 6 to 12.
- To the best of our knowledge, a master-slave Kalman filter is proposed for the first time to solve this new estimation problem.
- In order to increase the observability of the new state vector, the measurement vector of the master estimator (EKF) is also extended by using angular velocities and accelerations estimated by the slave estimator (inverse Φ).

- The performance of the proposed fusion algorithm is compared to Newton Predictor Enhanced Kalman Filter (NPEKF) [25] that provides estimates of the angular accelerations.
- In literature, error state Kalman filter (ErKF) [9, 10] has not been used to estimate angular accelerations. In this work, ErKF is also implemented as the master estimator to estimate the state vector. Both EKF and ErKF are found to have comparable performance.

The proposed filter has some advantages compared to the existing work in the literature. When the performance of the proposed algorithm is compared to NPEKF, the simulation results show that the master-slave algorithm outperforms the NPEKF. Smoother pitch and yaw accelerations are obtained by the proposed method.

The remainder of this paper is organized as follows: Section 2 presents modeling of the inertial sensors (IMU) and details the architecture of the master-slave Kalman filter algorithm. Section 3 describes modeling of the 2-DOF pan-tilt platform. In Section 4, acceleration controllers for both pan and tilt axes are designed using the inner acceleration control technique. Section 5 presents simulation results to validate the effectiveness of the proposed angular acceleration estimation algorithm by using the estimated inertial accelerations as feedback signals in the stabilization control of the 2-DOF pan-tilt system. Simulation results that compare the performance of the proposed algorithm with the NPEKF and ErKF are also provided. Finally, Section 6 concludes the paper with some remarks and indicates possible future directions.

2 Sensor Modeling and Sensor Fusion by a Master-Slave Kalman Filter

Modeling of MEMS inertial sensors and the proposed sensor fusion algorithm are presented in this section.

2.1 Sensor Modeling

MEMS inertial sensors (gyroscopes, accelerometers and magnetometers) are modeled by corrupting the true sensor measurements with sensor errors. In practice, due to their mechanical and electrical natures, MEMS inertial sensors are frequently mixed with

two types of errors: deterministic and stochastic errors [29]. Deterministic errors mostly include stable and repeatable biases, which can be eliminated through some suitable calibration. However, stochastic errors are based on multiplicative or additive measurement noises that can not be eliminated via simple calibration. In this work, random noises are assumed to be drawn from a normal distribution.

2.1.1 Gyroscope

Gyroscopes measure angular rates in the body frame. The gyroscope output can be modeled as:

$$\omega_g^b = \omega_0^b + b_g + \eta_g \quad (1)$$

where $\omega_0^b = [\omega_{x_0}^b \ \omega_{y_0}^b \ \omega_{z_0}^b]^T$ defines the true rotation rates in the body frame, b_g and η_g represent the gyro biases and noises.

2.1.2 Accelerometer

Accelerometers measure specific forces in the body frame. These forces are the total accelerations relative to free-fall and represented by f_a . It is assumed that IMU is attached to the body center and earth rotation effects are neglected. Then, the true specific forces are computed in the inertial frame as follows:

$$f_0^n = \dot{V}^n + g, \quad g = \begin{bmatrix} 0 \\ 0 \\ -9.81 \end{bmatrix} \quad (2)$$

where \dot{V}^n denotes a vector of the translational accelerations of the body and g is the acceleration due to gravity. Since accelerometers measure the specific forces in the body frame, f_0^n is multiplied by the rotation matrix, R_n^b , to transform from *inertial* to *body* frame as shown in (3).

$$f_0^b = R_n^b f_0^n = R_n^b \dot{V}^n + R_n^b g \quad (3)$$

The rotation matrix from the inertial frame to the body frame, R_n^b , is computed using XYZ convention of the Euler angles. Specifically, the first rotation is about X axis by a roll angle ϕ , which is denoted as $R_x(\phi)$. The second rotation, $R_y(\theta)$, is about Y axis by a pitch angle θ . Finally, the third rotation, $R_z(\psi)$, is about Z axis by a yaw angle ψ . Then the rotation matrix

is computed by the product of these transformation matrices as follows:

$$\begin{aligned} R_n^b &= R_x(\phi)R_y(\theta)R_z(\psi) \\ &= \begin{bmatrix} \cos\psi\cos\theta & \cos\theta\sin\psi & -\sin\theta \\ \cos\psi\sin\phi\sin\theta - \cos\phi\sin\psi & \cos\phi\cos\psi + \sin\phi\sin\psi\sin\theta & \cos\theta\sin\phi \\ \sin\phi\sin\psi + \cos\phi\cos\psi\sin\theta & \cos\phi\sin\psi\sin\theta - \cos\psi\sin\phi & \cos\psi\cos\theta \end{bmatrix} \end{aligned} \quad (4)$$

where

$$\begin{aligned} R_x(\phi) &= \begin{bmatrix} 1 & 0 & 0 \\ 0 & \cos\phi & \sin\phi \\ 0 & -\sin\phi & \cos\phi \end{bmatrix}, \\ R_y(\theta) &= \begin{bmatrix} \cos\theta & 0 & -\sin\theta \\ 0 & 1 & 0 \\ \sin\theta & 0 & \cos\theta \end{bmatrix}, \end{aligned}$$

and,

$$R_z(\psi) = \begin{bmatrix} \cos\psi & \sin\psi & 0 \\ -\sin\psi & \cos\psi & 0 \\ 0 & 0 & 1 \end{bmatrix}$$

Usually V^n is assumed to be constant and therefore $\dot{V}^n = 0$. Then, (3) is expressed as:

$$f_0^b = R_n^b g = \begin{bmatrix} -g\sin\theta \\ g\cos\theta\sin\phi \\ g\cos\phi\cos\theta \end{bmatrix} \quad (5)$$

where ϕ and θ are the roll and pitch angles. The output of the accelerometer is modeled as:

$$f_a^b = f_0^b + b_a + \eta_a \quad (6)$$

where b_a and η_a define the accelerometer biases and noises.

2.1.3 Magnetometer

Magnetometers measure the strength of the magnetic fields in the body frame. The magnetometer output is modeled as:

$$H_m^b = H_0^b + b_m + \eta_m \quad (7)$$

where H_0^b defines the true magnetometer measurements in the body frame, b_m and η_m represent the magnetometer biases and noises.

2.2 Sensor Fusion by a Master-Slave Kalman Filter

Conventional sensor fusion methods based on Kalman filter estimate Euler angles and the gyroscope biases [30, 31]. The state vector is defined as follows:

$$x = [\phi \ \theta \ \psi \ b_{gx} \ b_{gy} \ b_{gz}]^T = [\Theta^T \ b_g^T]^T \quad (8)$$

where $\Theta \equiv [\phi \ \theta \ \psi]^T$ represent Euler angles (roll, pitch and yaw) and the gyroscope biases are denoted by $b_g \equiv [b_{gx} \ b_{gy} \ b_{gz}]^T$. The nonlinear process dynamics is described by the following kinematic relationship between the Euler rates $\Omega = [\dot{\phi} \ \dot{\theta} \ \dot{\psi}]^T$ and the angular velocity vector $\omega = [\omega_x \ \omega_y \ \omega_z]^T$ [32] :

$$\Omega = \mathbb{B}\omega \quad (9)$$

where \mathbb{B} is the velocity transformation matrix and defined as:

$$\mathbb{B} = \begin{bmatrix} 1 & \sin\phi\tan\theta & \cos\phi\tan\theta \\ 0 & \cos\theta & -\sin\phi \\ 0 & \sin\phi\sec\theta & \cos\phi\sec\theta \end{bmatrix} \quad (10)$$

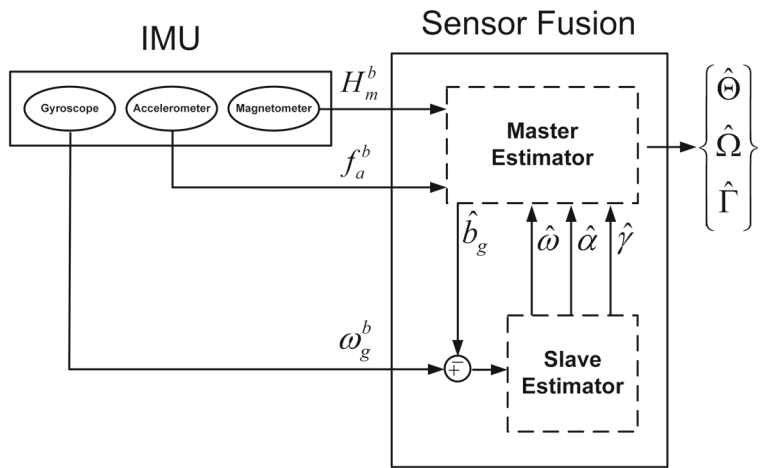
The velocity transformation matrix, \mathbb{B} , given by (10) becomes singular when $\theta = \pi/2$ because $\tan\theta = \infty$ or $\sec\theta = \infty$ at $\theta = \pi/2$. In this work, the tilt axis is constrained to be in the range ($[0, \pi/2]$), and therefore there is no "gimbal lock" problem! We should remark that the choice of Euler angles or quaternions is a matter of preference, and due to its simplicity Euler angles are preferred. The state vector in (8) is extended to include angular velocities and accelerations; i.e.

$$\begin{aligned} X &= [\phi \ \theta \ \psi \ \dot{\phi} \ \dot{\theta} \ \dot{\psi} \ \ddot{\phi} \ \ddot{\theta} \ \ddot{\psi} \ b_{gx} \ b_{gy} \ b_{gz}]^T \\ &= [\Theta^T \ \Omega^T \ \Gamma^T \ b^T]^T \end{aligned} \quad (11)$$

where $\Gamma \equiv [\ddot{\phi} \ \ddot{\theta} \ \ddot{\psi}]^T$ defines Euler accelerations.

In accordance with the new state vector (11), the following continuous-time process dynamics is

Fig. 1 Block diagram of the master-slave Kalman filter



obtained by differentiating the nonlinear dynamics in (9):

$$\frac{d}{dt}X = \begin{bmatrix} \dot{\Theta} \\ \dot{\Omega} \\ \dot{\Gamma} \\ \dot{b}_g \end{bmatrix} = \begin{bmatrix} \mathbb{B}\omega \\ \dot{\mathbb{B}}\omega + \mathbb{B}\alpha \\ \ddot{\mathbb{B}}\omega + 2\dot{\mathbb{B}}\alpha + \mathbb{B}\gamma \\ 0_{3 \times 1} \end{bmatrix} + W \quad (12)$$

where angular accelerations and jerks are denoted by $\dot{\omega} \equiv \alpha = [\alpha_x \alpha_y \alpha_z]^T$ and $\dot{\alpha} \equiv \gamma = [\gamma_x \gamma_y \gamma_z]^T$ in the body coordinate frame. Non-deterministic effects and modeling errors are represented by the process noise, W . In (12), gyro biases are assumed to be constant. This model is known as a *Wiener process* and can be considered as a special case of *Gauss-Markov process* [33].

Remark 1 Gyro biases can also be modeled using *Singer Model*. This model assumes that the gyro bias is a zero-mean stationary *first order Markov process* [28]. The continuous time bias model is defined as:

$$\dot{b}_g = -\beta b_g + w \quad (13)$$

where w is a zero mean white noise and β is the reciprocal of the time constant. Note that $\beta = 0$ implies constant bias model.

To estimate the state vector X in (11), an extended Kalman filter that utilizes sensor measurements was implemented. To run the EKF, we need to compute ω , α and γ that appear on the right hand side of (12).

Since there are no additional sensors to measure angular accelerations and jerks, they need to be estimated from gyro measurements. To this end, a slave type inverse Φ -algorithm is introduced to estimate ω , α and γ using bias compensated gyro readings. Since biases will be estimated by EKF and used as inputs to the inverse Φ -algorithm, we have a master-slave configuration in Fig. 1 where the master estimator feeds the slave estimator with bias estimates and the slave estimator returns estimated angular velocity, accelerations and jerks to the master estimator.

2.2.1 Master Estimator

Process dynamics of the master estimator is given by (12). Applying Euler's forward discretization to the process dynamics leads to:

$$\begin{bmatrix} \Theta \\ \Omega \\ \Gamma \\ b_g \end{bmatrix}_{k+1} = \begin{bmatrix} \Theta \\ \Omega \\ \Gamma \\ b_g \end{bmatrix}_k + T \begin{bmatrix} \mathbb{B}\omega \\ \mathbb{F}\omega + \mathbb{B}\alpha \\ \mathbb{H}\omega + 2\mathbb{F}\alpha + \mathbb{B}\gamma \\ 0_{3 \times 1} \end{bmatrix}_k + W_k \quad (14)$$

where $\mathbb{F} \equiv \dot{\mathbb{B}}$, $\mathbb{H} \equiv \dot{\mathbb{F}} = \ddot{\mathbb{B}}$, T is the sampling period and W_k is the white Gaussian process noise with zero mean. Measurement vector of the master estimator contains the specific force measurements, f_a^b , from accelerometer and the yaw angle, ψ_m , determined from the resolved components of the magnetic field measurements, H_m^b , in the horizontal plane along

the heading axis [34]. In order to increase the observability of the state vector, the measurement vector of EKF is also extended by using angular velocities, $\hat{\omega}$, and accelerations, $\hat{\alpha}$ estimated by the slave filter:

$$Y_k = [f_a^b \ \psi_m \ \hat{\omega} \ \hat{\alpha}]_k^T = \begin{bmatrix} R_n^b(\Theta)g \\ \psi \\ \mathbb{E}\Omega \\ \mathbb{E}\Gamma + \mathbb{G}\Omega \end{bmatrix}_k + V_k \quad (15)$$

where V_k is the time correlated measurement noise [35]:

$$V_k = \Lambda_{k-1} V_{k-1} + \zeta_{k-1} \quad (16)$$

with $\Lambda_{k-1} = e^{-\frac{T}{\kappa}} I_{3 \times 3}$ is the transition matrix of the time correlated errors with the time constant, κ , ζ_{k-1} represents the white Gaussian noise with zero mean, R_n^b is the rotation matrix from the inertial frame to the body frame in (4), $\mathbb{G} = \dot{\mathbb{E}}$, g is the gravitational acceleration vector and the inverse velocity transformation matrix, \mathbb{E} , is defined as:

$$\mathbb{E} = \mathbb{B}^{-1} = \begin{bmatrix} 1 & 0 & \sin \theta \\ 0 & \cos \phi & \cos \theta \sin \phi \\ 0 & -\sin \phi & \cos \phi \cos \theta \end{bmatrix} \quad (17)$$

As it is seen from (14) and (15), the process and measurement models of the master estimator are nonlinear so EKF will be implemented to estimate the state vector X .

Remark 2 Larger the time constant leads to more correlated measurement noises. If κ approaches infinity, then the transition matrix becomes identity and $V_k = V_{k-1} + \zeta_{k-1}$, i.e. the measurement noises are time correlated. On the other hand, if the time constant is small, the measurement noises are less correlated and they behave like a white Gaussian noise with zero mean, i.e. $V_k = \zeta_{k-1}$.

2.2.2 Slave Estimator

The slave estimator provides estimates of angular velocities, accelerations and jerks to the master estimator. The following process dynamics is constructed in discrete time, based on the classical laws of motion using Taylor series where angular jerks are assumed to be constant:

$$\begin{bmatrix} \omega \\ \alpha \\ \gamma \end{bmatrix}_{k+1} = \begin{bmatrix} I_{3 \times 3} & TI_{3 \times 3} & 0.5T^2 I_{3 \times 3} \\ 0_{3 \times 3} & I_{3 \times 3} & TI_{3 \times 3} \\ 0_{3 \times 3} & 0_{3 \times 3} & I_{3 \times 3} \end{bmatrix} \begin{bmatrix} \omega \\ \alpha \\ \gamma \end{bmatrix}_k + \mathbb{W}_k \quad (18)$$

where T is the sampling period and \mathbb{W}_k is the white Gaussian process noise with zero mean. The gyro bias estimated by the EKF is subtracted from the gyro readings to obtain bias compensated body angular velocity, $\omega_g^b - \hat{\omega}_g = [\omega_{gx}^b - \hat{\omega}_{gx}, \omega_{gy}^b - \hat{\omega}_{gy}, \omega_{gz}^b - \hat{\omega}_{gz}]^T$, which is used as the measurement for the slave estimator:

$$\mathbb{Y}_k = \omega_g^b - \hat{\omega}_g = [I_{3 \times 3} \ 0_{3 \times 6}] \begin{bmatrix} \omega \\ \alpha \\ \gamma \end{bmatrix}_k + \mathbb{V}_k \quad (19)$$

where \mathbb{V}_k is the time correlated measurement noise [35]:

$$\mathbb{V}_k = \lambda_{k-1} \mathbb{V}_{k-1} + \xi_{k-1} \quad (20)$$

with $\lambda_{k-1} = e^{-\frac{T}{\kappa}} I_{3 \times 3}$ is the transition matrix of the time correlated errors with the time constant, κ , and ξ_{k-1} is the white Gaussian noise with zero mean. When the measurement errors at different times are highly correlated, the classical Kalman filter provides an approximate solution to the estimation problem because R_k is the covariance matrix of only ξ_k , not \mathbb{V}_k , i.e. $\xi_k \sim N(0, R_k)$. Bryson and Henrikson [36] proposed a time-differencing algorithm also known as an *Inverse R-Algorithm* in order to handle with time correlated measurement errors. However, this algorithm introduces one step delay because the computation of apriori state estimate must use the current measurement. To resolve this problem, Petovello et al. [37, 38] proposed a revised time-differencing algorithm which is known as an *Inverse Φ-Algorithm*. We employ the inverse Φ-algorithm to estimate angular velocity (ω), acceleration (α) and jerk (γ) using process and measurement models given by (18)–(20), respectively. The prediction stage of the inverse Φ-algorithm is the same with the prediction step of the Kalman filter. On the other hand, the update stage of the inverse Φ-algorithm is modified based on Kalman filter. The prediction and update stages of the inverse Φ-algorithm are presented in the Appendix [35].

3 Modeling of the Pan-Tilt Platform

Dynamical model of the 2 DOF pan-tilt platform in Fig. 2 is presented in this section.

The nonlinear model of the pan-tilt system based on the Euler-Lagrange formulation is as follows [39]:

$$D(q)\ddot{q} + C(q, \dot{q})\dot{q} + G(q) + F(\dot{q}) = \tau + \tau_d \quad (21)$$

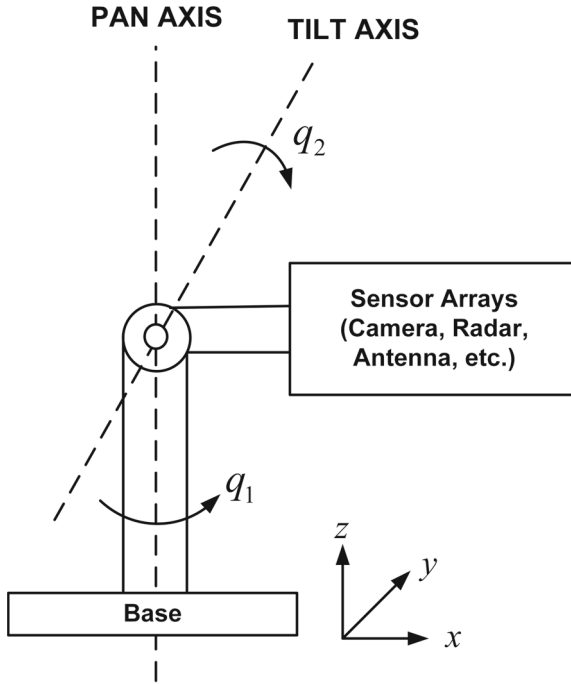


Fig. 2 Pan-tilt mechanism

where

$$\begin{aligned}
 q &= [q_1 \ q_2]^T, \quad \tau = [\tau_1 \ \tau_2]^T \\
 D(q) &= \begin{bmatrix} D_{11} & D_{12} \\ D_{21} & D_{22} \end{bmatrix}, \quad C(q, \dot{q}) = \begin{bmatrix} C_{11} & C_{12} \\ C_{21} & C_{22} \end{bmatrix} \\
 G(q) &= [0 \ 0.5gm_2l_2 \cos q_2]^T \\
 F(\ddot{q}) &= [v_1\dot{q}_1 + k_1\text{sgn}(\dot{q}_1) \ v_2\dot{q}_2 + k_2\text{sgn}(\dot{q}_2)]^T \\
 D_{11} &= \frac{1}{2}m_1l_1^2 + m_2l_1^2 + m_2l_1l_2 \cos q_2 + \frac{1}{3}m_2l_2^2 \cos^2 q_2 + J_1 \\
 D_{22} &= \frac{1}{3}m_2l_2^2 + J_2, \quad D_{12} = D_{21} = 0 \\
 C_{11} &= -m_2l_1l_2\dot{q}_2 \sin q_2, \quad C_{12} = -\frac{1}{3}m_2l_2^2\dot{q}_1 \sin 2q_2 \\
 C_{21} &= \dot{q}_1 \left(\frac{1}{2}m_2l_1l_2 \sin q_2 + \frac{1}{6}m_2l_2^2 \sin 2q_2 \right), \quad C_{22} = 0
 \end{aligned}$$

where $D(q)$ is the mass-inertia matrix, $C(q, \dot{q})$ defines centrifugal and Coriolis terms, $G(q)$ is the gravity vector, $F(\ddot{q})$ represents viscous and Coulomb frictions, τ is the control input vector, τ_d defines the unknown disturbances acting on both azimuth and elevation axes, and q , \dot{q} and \ddot{q} are the vectors of joint angles, velocities and accelerations, respectively. J_1 and J_2 are motor inertias, m_1 and m_2 are the masses of pan and tilt mechanisms, l_1 is the radius, l_2 is the

length, v_1 and v_2 are viscous friction coefficients, and k_1 and k_2 are Coulomb friction coefficients.

4 Stabilization Control Using Acceleration Feedback

The aim of stabilization control is to maintain the desired orientation by rejecting external disturbances. Figure 3 depicts the block diagram of stabilization control. $\Omega_c = 0$ and Ω are the velocity command and measured velocity, e_Ω is the velocity error, V_c is the voltage applied to the motor, τ is the control input torque and τ_d represents the unknown disturbances acting on both azimuth and elevation axes. Since Ω is fed by a gyroscope, stabilization is also referred as gyro stabilization. Velocity controller is designed as a PI controller to follow the velocity command as closely as possible.

The pan-tilt system converges from an initial orientation to the desired one by utilizing a PID position controller as shown in Fig. 4. Θ_{ref} and Ω_{ref} are reference Euler angles and rates, $\hat{\Theta}$ and $\hat{\Omega}$ are estimated Euler angles and rates, and e_Θ defines the position error. Since both orientation and velocity information are used as feedback in the position controller, an IMU is needed to perform sensor fusion.

Stabilization control loop can be improved by using acceleration feedback in a PI current controller to achieve high precision stabilization as shown in Fig. 5. J is the nominal inertia, K_T is the motor torque constant, K_β is the acceleration feedback gain, I_{ref} and \hat{I} represent reference and estimated currents, and e_I is the current error.

It is assumed that the center of rotation and the center of gravity of the pan-tilt mechanism are coincident. In the light of this assumption, the nonlinear pan-tilt system which is given by (21) is decoupled along the azimuth and elevation axes. Therefore, two separate linear controllers are designed for these axes. In this work, the inner acceleration control approach detailed in [40] and [41] is implemented as depicted in Fig. 5. The goal of acceleration control is to improve the stabilization performance of the pan-tilt system by rejecting external disturbances. The position loop produces reference signals for the velocity loop, which in turn creates reference signals for the current loop. Reliable angular acceleration signals estimated by the master-slave Kalman filter are used as feedback in

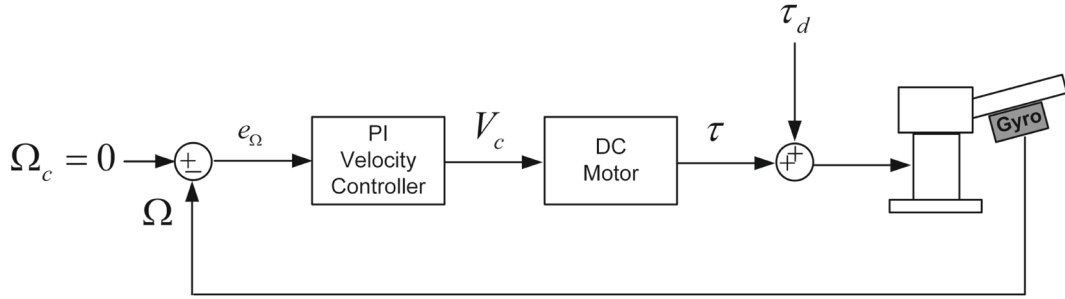


Fig. 3 Block diagram of stabilization control

the current controller because the success of stabilization control largely depends on reliable acceleration feedback. However, estimated accelerations are not directly utilized in the current controller. On the other hand, estimated currents that are directly used in the controller can be computed using the estimated accelerations based on the following idea. When a torque is exerted on an object, it begins to rotate with an angular acceleration inversely proportional to its moment of inertia. This relation can be defined as $\tau = J\Gamma$. Also, the torque is directly proportional to the current in the armature windings of the rotor so it can be computed as $\tau = K_T I$. Using these relationships, estimated currents are calculated as $\hat{I} = \frac{J\hat{\Gamma}}{K_T}$ where $\hat{\Gamma}$ is the estimated angular acceleration. Then, the estimated current is scaled by the acceleration feedback gain, K_β , and used as feedback signals in the current controller.

Acceleration control is effective in disturbance rejection because the effects of disturbance will be sensed first in the acceleration signal before a significant velocity error can build up in the velocity loop. Higher acceleration gain adds more electronic inertia to the physical inertia of the total system [42]. Thus, the overall system exhibits high dynamic stiffness and

has better disturbance rejection. The increase in effective inertia reduces the speed of the system's response. In order to preserve the loop gain, one should scale up the control loop gains by the factor $(1 + K_\beta)$ as in Fig. 5.

The following PID controllers generate reference velocities for the velocity control loops for the azimuth and elevation axes:

$$\dot{\psi}_{ref} = K_{P_\psi} e_\psi + K_{I_\psi} \int e_\psi dt + K_{D_\psi} \dot{e}_\psi \quad (22)$$

$$\dot{\theta}_{ref} = K_{P_\theta} e_\theta + K_{I_\theta} \int e_\theta dt + K_{D_\theta} \dot{e}_\theta \quad (23)$$

where the orientation errors in the azimuth and elevation axes are defined respectively as follows:

$$e_\psi = \psi_{ref} - \hat{\psi} \quad (24)$$

$$e_\theta = \theta_{ref} - \hat{\theta} \quad (25)$$

Velocity and current controls are designed as PI controllers for the azimuth and elevation axes. Reference currents for the azimuth and elevation axes are generated as follows:

$$I_{ref1} = (1 + K_{\beta_1}) K_{P_\psi} e_\psi + (1 + K_{\beta_1}) K_{I_\psi} \int e_\psi dt \quad (26)$$

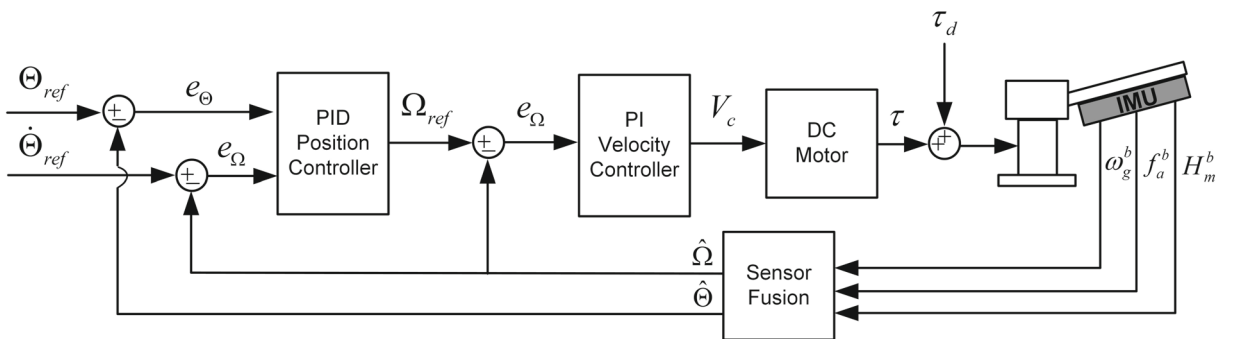


Fig. 4 Block diagram of stabilization control with PID position control

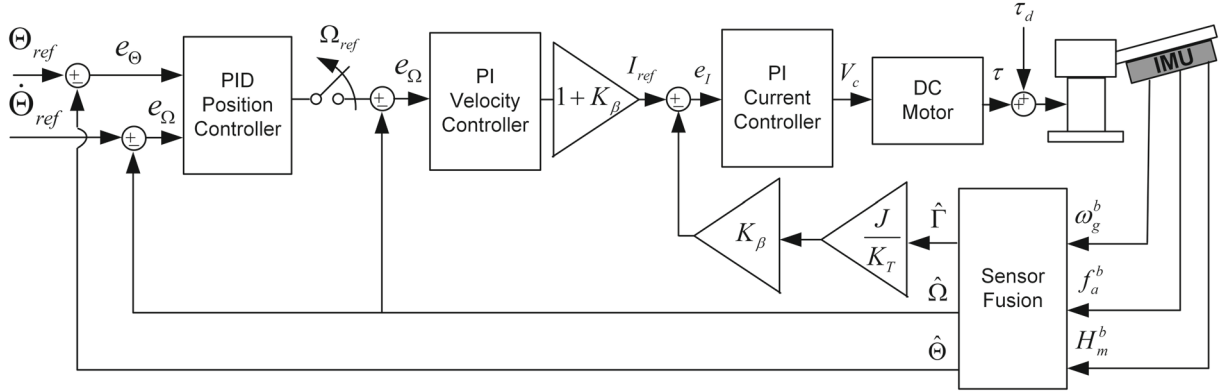


Fig. 5 Block diagram of acceleration feedback control

$$I_{ref_2} = (1 + K_{\beta_2})K_{P_\beta}e_{\dot{\theta}} + (1 + K_{\beta_2})K_{I_{\dot{\theta}}}\int e_{\dot{\theta}}dt \quad (27)$$

where

$$e_{\dot{\psi}} = \dot{\psi}_{ref} - \hat{\dot{\psi}} \quad (28)$$

$$e_{\dot{\theta}} = \dot{\theta}_{ref} - \hat{\dot{\theta}} \quad (29)$$

where $e_{\dot{\psi}}$ and $e_{\dot{\theta}}$ represent the velocity errors in the azimuth and elevation axes, respectively. Finally, torque control inputs are designed for the azimuth and elevation axes as follows:

$$\tau_1 = K_{P_1}e_{I_1} + K_{I_1}\int e_{I_1}dt \quad (30)$$

$$\tau_2 = K_{P_2}e_{I_2} + K_{I_2}\int e_{I_2}dt \quad (31)$$

where the current errors in the azimuth and elevation axes are defined as:

$$e_{I_1} = I_{ref_1} - \hat{I}_1 \quad (32)$$

$$e_{I_2} = I_{ref_2} - \hat{I}_2 \quad (33)$$

5 Simulation Results

Simulation results for two different scenarios are presented in this section where the proposed estimation algorithm is incorporated into a high fidelity simulation model to test the stabilization performance of the pan-tilt system subject to various external disturbances. In order to construct a high fidelity simulation model, both nonlinear dynamics of the pan-tilt platform given by (21) and realistic sensor models given by (1), (6), (7) are utilized. Biases and noises that

corrupt sensor outputs are tabulated in Table 1 where SNR denotes signal to noise ratio. The update rates of MEMS inertial sensors that are provided in Table 1 are selected based on the specifications given in the inertial sensor market¹. Since we assume that EKF and the inverse Φ-algorithm run at 1000 Hz, the proposed sensor fusion algorithm executes faster than these inertial sensors. Therefore, the master-slave Kalman filter algorithm may generate estimates before one of the gyroscope, accelerometer and magnetometer measurements are completed.

The quality of the estimated signals with the incomplete measurements due to the different rates for the MEMS inertial sensors will be deteriorated if proper action is not taken. This leads to the loss of data integrity. In order to ensure data integrity, we add a rate transition block at the output of each sensor in the simulations. We use this rate transition as a double buffer. The gyroscope provides angular velocity measurements to the slave estimator. When the gyro measurement is obtained, this data is transferred to the first buffer. The slave estimator takes the gyro data from this buffer until a new measurement is available. When a new gyro measurement is available, it is saved to the second buffer, the buffer index is changed, and the new measurement is used by the inverse Φ-algorithm. Similar double buffers are also used for accelerometer and magnetometer.

The reference trajectories in the inertial frame are selected to be smooth step functions of time in the simulations. Once the system reaches the target orientation, the PID position controller is deactivated

¹Advanced Navigation, Spatial FOG (GPS aided INS and AHRS)

Table 1 Simulation Parameters

Parameter	Description	Value
m_1	Pan mass	75 kg
m_2	Tilt mass	50 kg
L_1	Pan radius	0.5 m
L_2	Tilt length	0.7 m
$J_{1,2}$	Motor inertias	$2 \times 10^{-2} \text{ kg.m}^2$
K_t	Motor torque constant	$6.87 \times 10^{-2} \text{ N.m}/\sqrt{\text{W}}$
Bw_g	Bandwidth of gyro	440 Hz
Bw_a	Bandwidth of accelerometer	200 Hz
Bw_m	Bandwidth of magnetometer	110 Hz
b_g	Gyro bias	$[1 - 1 0.5]^T \text{ deg/s}$
b_a	Accelerometer bias	$[0.01 - 0.01 0.005]^T \text{ g}$
b_m	Magnetometer bias	$[0.01 - 0.01 0.02]^T \text{ Wb/m}^2$
S_{η_g}	SNR of gyro	65 dB
S_{η_a}	SNR of accelerometer	45 dB
S_{η_m}	SNR of magnetometer	61 dB

and the reference velocity becomes zero, $\Omega_{ref} = 0$, as shown in Fig. 5. Thus, the pan-tilt system is stabilized by the PI velocity controller instead of PID position controller. Since the goal is to improve robustness of the stabilized pan-tilt system under external disturbances, acceleration feedback is introduced into the PI current controller. External disturbances are applied to the system to mimic realistic conditions in both scenarios. When the external disturbances are discarded, PID controller is not activated but the velocity controller is still utilized. The time synchronization between EKF and the inverse Φ -algorithm is achieved by introducing a unit delay to the output of EKF. The inverse Φ -algorithm uses the inverse of the state transition matrix. Thus, this algorithm produces stable and converging estimates if the transition matrix is not ill-conditioned. Since EKF is based on the linearization of nonlinear models given by (14)–(16), convergence is not guaranteed; however, by the proper choice of process and measurement noise covariance matrices, Q and R , and by increasing the observability of the state vector, one usually achieves stable filter operation with good convergence. In simulations, the filter parameters (Q and R) are tuned as follows:

$$Q_{master} = \begin{bmatrix} 10I_{3 \times 3} & 0_{3 \times 3} & 0_{3 \times 3} & 0_{3 \times 3} \\ 0_{3 \times 3} & 11I_{3 \times 3} & 0_{3 \times 3} & 0_{3 \times 3} \\ 0_{3 \times 6} & 0_{3 \times 3} & 12I_{3 \times 3} & 0_{3 \times 3} \\ 0_{3 \times 3} & 0_{3 \times 3} & 0_{3 \times 3} & 13I_{3 \times 3} \end{bmatrix},$$

$$R_{master} = \begin{bmatrix} 10^{-4}I_{4 \times 4} & 0_{4 \times 6} \\ 0_{6 \times 4} & 10^{-3}I_{6 \times 6} \end{bmatrix}$$

$$Q_{slave} = \begin{bmatrix} I_{3 \times 3} & 0_{3 \times 3} & 0_{3 \times 3} \\ 0_{3 \times 3} & 2I_{3 \times 3} & 0_{3 \times 3} \\ 0_{3 \times 3} & 0_{3 \times 3} & 3I_{3 \times 3} \end{bmatrix}, \quad R_{slave} = 10^{-2}I_{3 \times 3}$$

where I and 0 represent the identity and zero matrices.

5.1 Results of the Proposed Fusion Algorithm

This section evaluates the performance of the proposed filter that employs both an extended Kalman filter (EKF) and an inverse Φ -algorithm in a master-slave configuration by using reliable angles, velocities and accelerations as feedback signals in the stabilization control of the pan-tilt system. Sections 5.1.1 and 5.1.2 present the first and second scenario results, respectively.

5.1.1 First Scenario

The pan-tilt platform is exposed to continuous, random and small amplitude disturbances. Figure 6 shows the disturbances applied to the azimuth and elevation axes. Gaussian distributed noises are used to generate these disturbances.

Azimuth and elevation angle responses are presented in Figs. 7 and 8, respectively. Desired values of azimuth and elevation references are 45 deg and 55 deg. When the acceleration feedback is not used in the current controller, oscillations occur in the azimuth angle response. The maximum overshoot from the

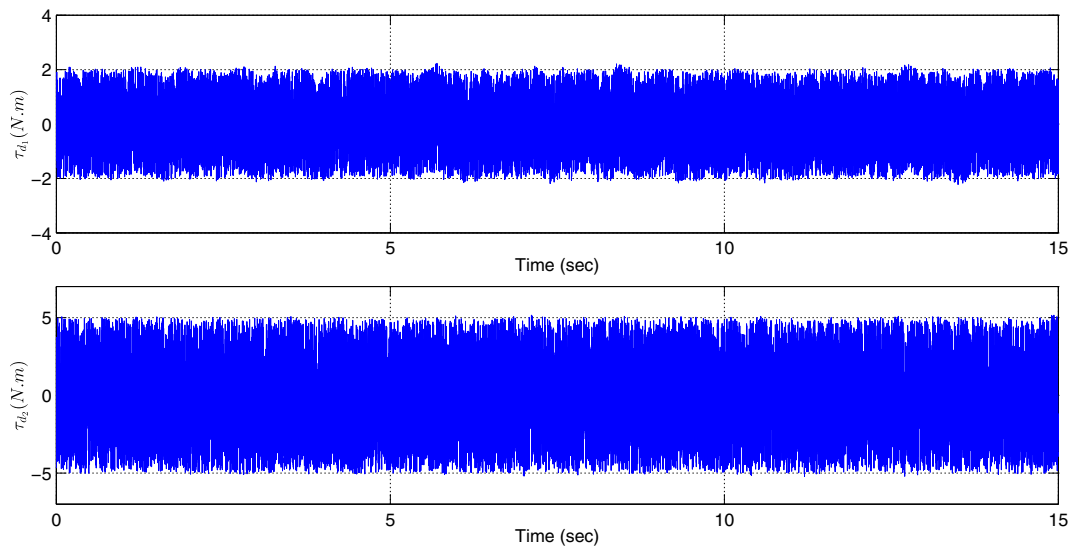


Fig. 6 External disturbances applied on the azimuth and elevation axes

Fig. 7 Azimuth angle responses

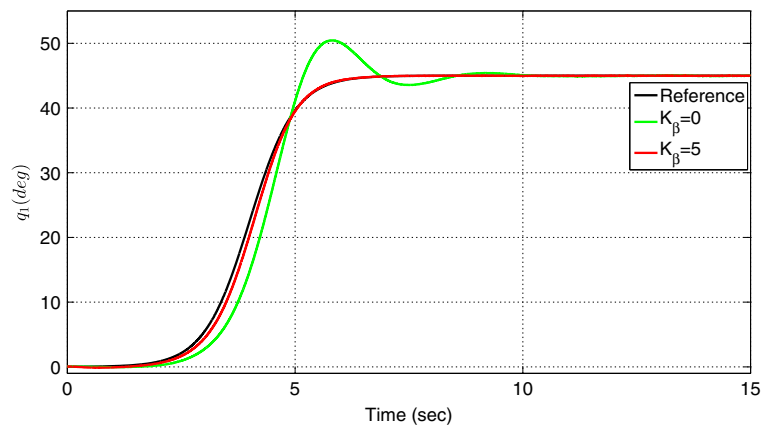
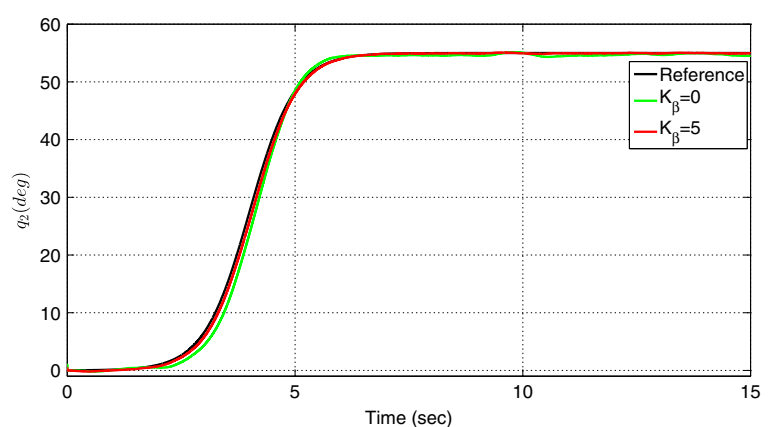


Fig. 8 Elevation angle responses



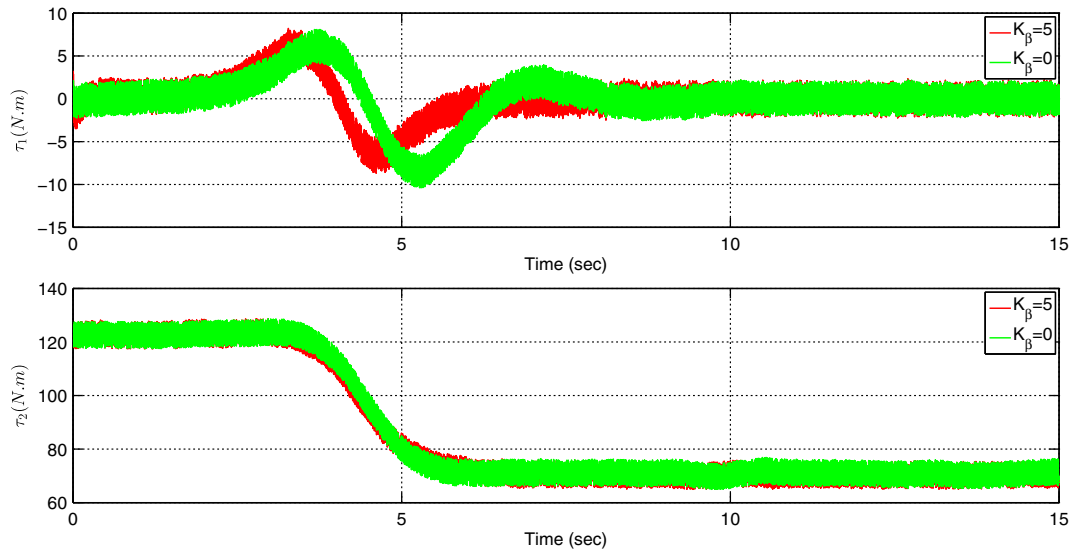


Fig. 9 Torque control inputs of the azimuth and elevation axes

azimuth angle response curve is about 12 %. On the other hand, the azimuth angle converges to the reference value in a smoother way when the acceleration feedback is introduced, e.g. $K_\beta = 5$. For the elevation angle response, the system does not exactly converge to 55 deg without the use of acceleration feedback. The elevation angle oscillates between 54.5 deg and 55.2 deg at the steady state. As the acceleration feedback is introduced, sufficiently small steady state error is achieved in the elevation angle response.

Figure 9 shows control efforts for $K_\beta = 0$ and $K_\beta = 5$. The amplitudes of the control inputs which are provided by the acceleration control are similar to those that are obtained without the use of acceleration feedback. RMS value of the control input for the azimuth axis is 2.83 N.m and slightly decreases

to 2.35 N.m with the use of acceleration feedback. When the acceleration feedback is used in the PI current control loop, RMS value of the control input changes from 89.47 N.m to 89.13 N.m for the elevation axis. These results show that acceleration control does not require larger control inputs to obtain better output angle responses when the system is exposed to continuous disturbances.

The master estimator which is implemented by using the EKF provides the estimates of pitch and yaw angles, velocities and accelerations based on (14)–(16). In Figs. 10 and 11, estimated Euler angles are provided. EKF performance is evaluated by RMS value of the errors between measured and estimated pitch and yaw angles. RMS values of the estimation errors of the pitch angle are 0.0057 deg and 0.0168

Fig. 10 Estimated pitch angles

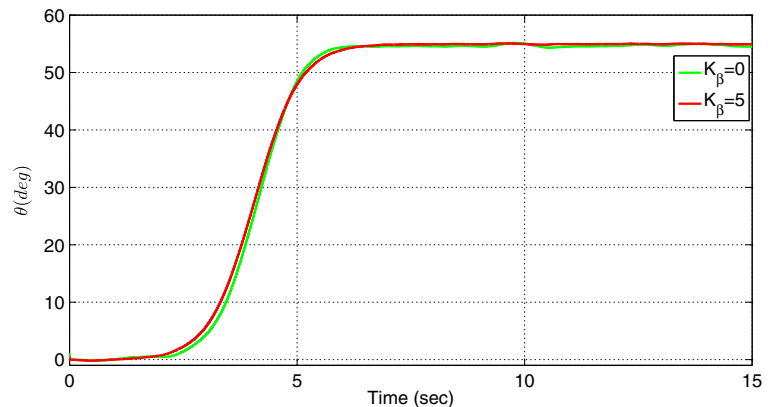


Fig. 11 Estimated yaw angles

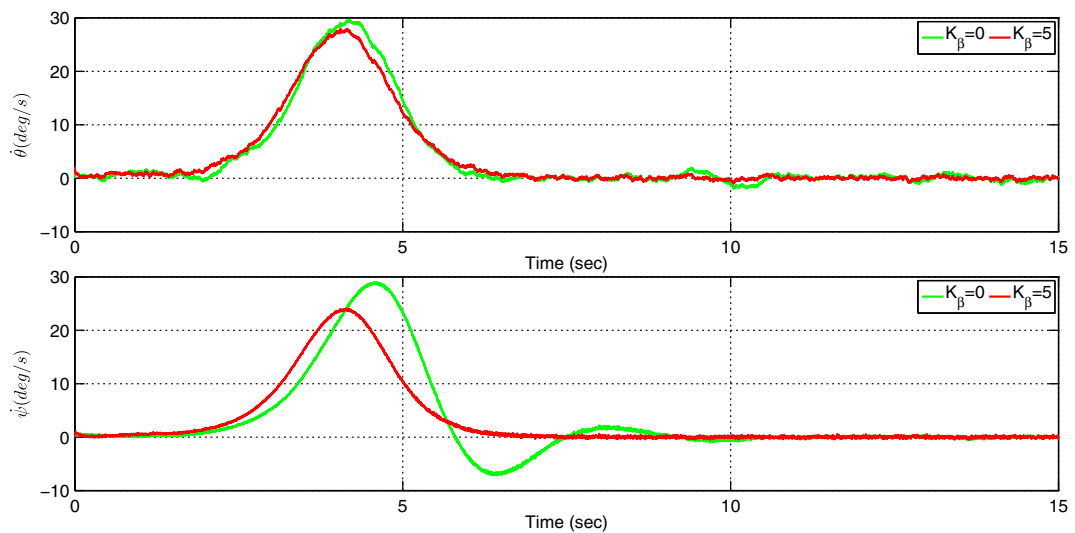
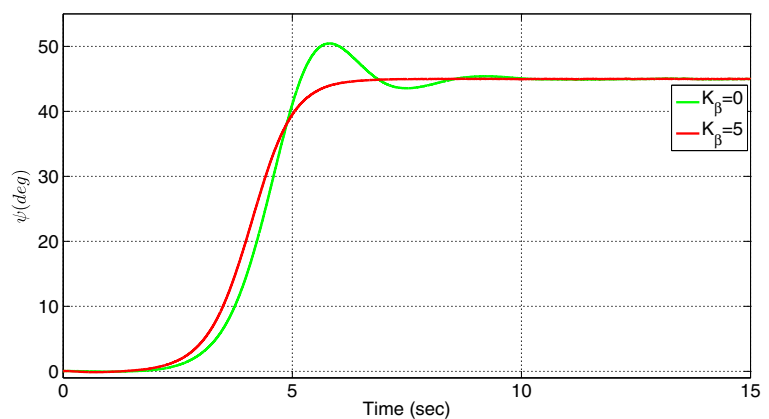


Fig. 12 Estimated Euler velocities

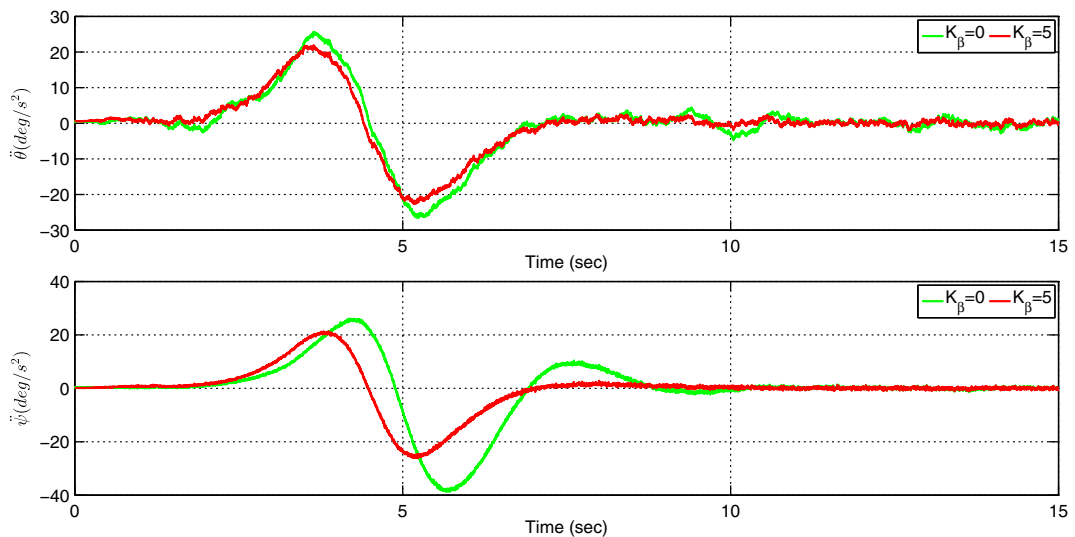


Fig. 13 Estimated Euler accelerations

Fig. 14 Estimated angular velocities about x axis

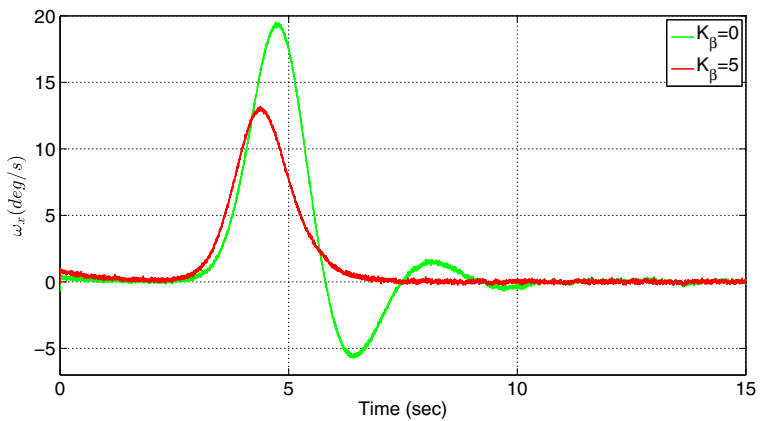


Fig. 15 Estimated angular velocities about y axis

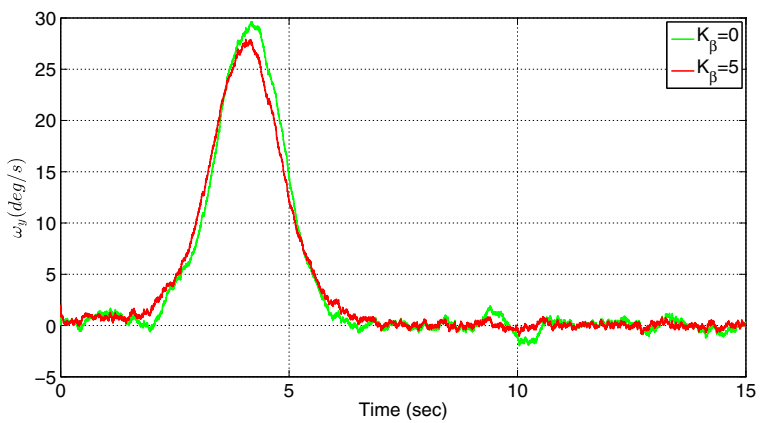
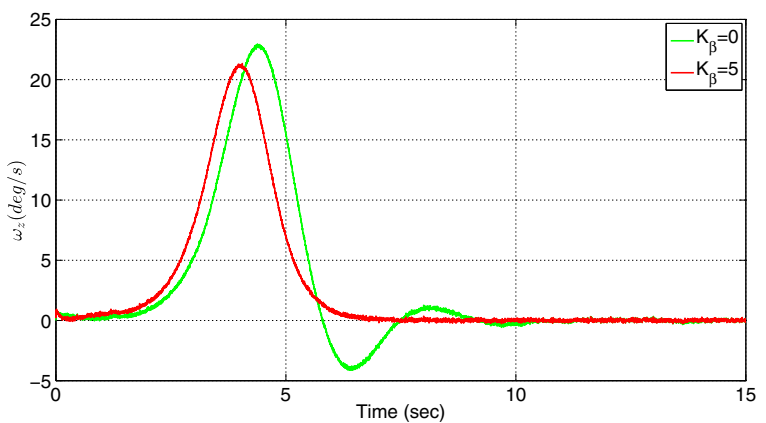


Fig. 16 Estimated angular velocities about z axis



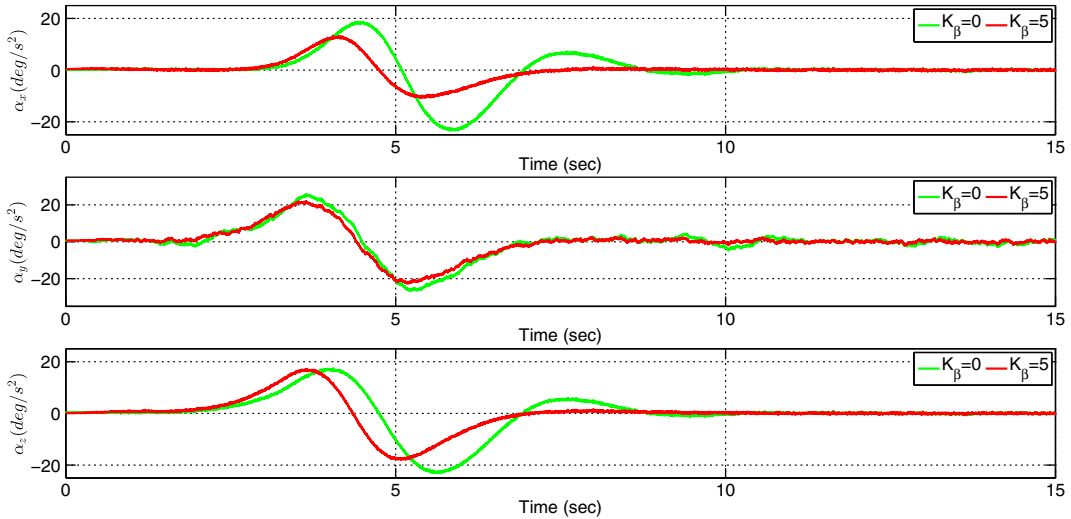


Fig. 17 Estimated angular accelerations

deg for $K_\beta = 0$ and $K_\beta = 5$, respectively. Also, RMS values of the estimation errors of the yaw angle are obtained as 4.48×10^{-7} deg and 4.66×10^{-7} deg for $K_\beta = 0$ and $K_\beta = 5$, respectively. Since all the estimation errors are small, estimated signals converge to measured values successfully for both $K_\beta = 0$ and $K_\beta = 5$. On the other hand, Euler velocities and accelerations are estimated as depicted in Figs. 12 and 13. The amplitude of oscillations are larger in both velocity and acceleration responses for $K_\beta = 0$ because the

angle responses are not smooth when the acceleration feedback is not utilized.

Angular velocities, accelerations and jerks are estimated by the slave filter using the process and measurement models in (18)–(20). When the acceleration feedback is utilized, small amplitude angular velocities are obtained in Figs. 14, 15 and 16. These results are not surprising because better angle responses are achieved with the use of acceleration feedback in the current controller. Similar observations can be also

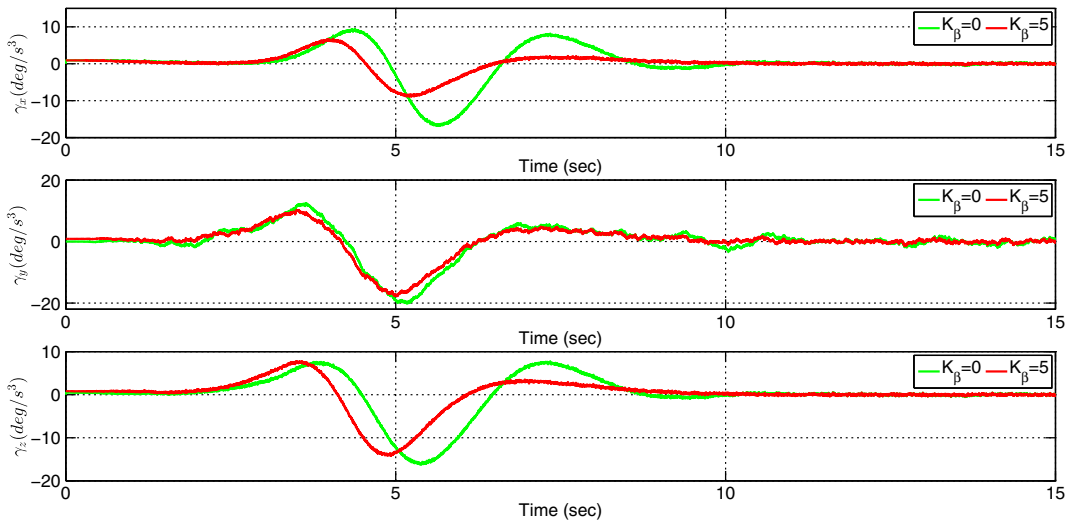


Fig. 18 Estimated angular jerks

done for estimated angular accelerations and jerks in Figs. 17 and 18.

5.1.2 Second Scenario

In the second scenario, the pan-tilt platform is exposed to sudden shocks after the desired positions are reached. In order to illustrate this case, disturbance torques are modeled as high amplitude step pulses with short durations. The amplitudes of the step pulses are assumed as 10 N.m and 15 N.m. Step disturbances are applied on the system between $t = 8$ sec and $t = 12$ sec as shown in Fig. 19. Figures 20 and 21 show the tracking performance for the azimuth and elevation axes. When the acceleration feedback is not used, azimuth and elevation angles cannot follow the reference trajectories successfully due to sudden shocks. The azimuth angle reaches to approximately 59 deg. When the acceleration feedback is used, small amplitude oscillations occur. Azimuth angle oscillates between 44.5 deg and 46 deg with the use of acceleration controller. In other words, azimuth angle is successfully stabilized despite the sudden shocks. Similar performances are also observed for the elevation angle responses. Smoother elevation angle response is achieved with the introduction of acceleration feedback. However, amplitudes of the oscillations increase to approximately 80 deg when the acceleration controller is not active.

In Fig. 22, control efforts are provided for $K_\beta = 0$ and $K_\beta = 12$. In order to reject the sudden shocks, large acceleration gain, $K_\beta = 12$, is used. As it is expected that when sudden shocks are not applied on the system, this acceleration gain leads to high amplitude oscillations compared to the case where acceleration feedback is not utilized. On the other hand, when sudden shocks are applied on the system, the amplitude of oscillations are larger without the use of acceleration feedback. As a result, pan and tilt axes is not stabilized due to sudden shocks even high control efforts are obtained for $K_\beta = 0$.

Similar to that of the first scenario, the master estimator is implemented by using the EKF based on (14)–(16). Figures 23 and 24 depict the estimated pitch and yaw angles. RMS values of the errors between the measured and estimated pitch angles are 0.0121 deg and 0.0095 deg for $K_\beta = 0$ and $K_\beta = 12$, respectively. On the other hand, RMS values of the errors between the measured and estimated yaw angles are 2.72×10^{-7} deg and 2.05×10^{-7} deg for $K_\beta = 0$ and $K_\beta = 12$. Since these errors are small, satisfactory estimates of pitch and yaw angles are obtained for both $K_\beta = 0$ and $K_\beta = 12$.

On the other hand, pitch and yaw velocities and accelerations are estimated as depicted in Figs. 25 and 26. When the acceleration controller is not active, high amplitude oscillations are observed in the estimated values as expected.

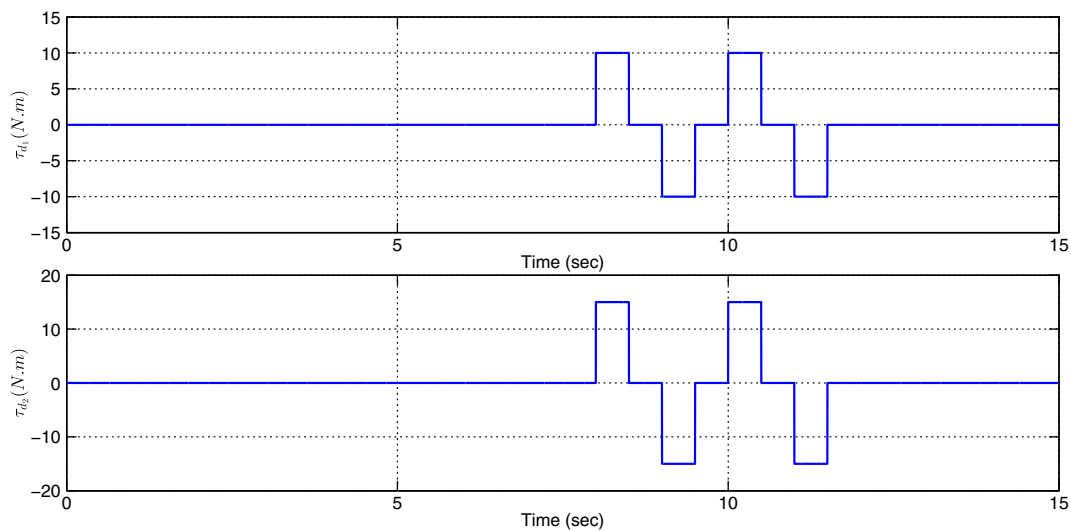


Fig. 19 External disturbances applied on the azimuth and elevation axes

Fig. 20 Azimuth angle responses

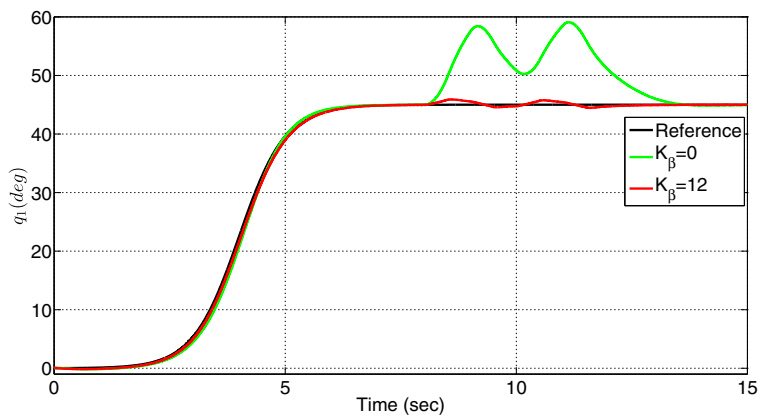


Fig. 21 Elevation angle responses

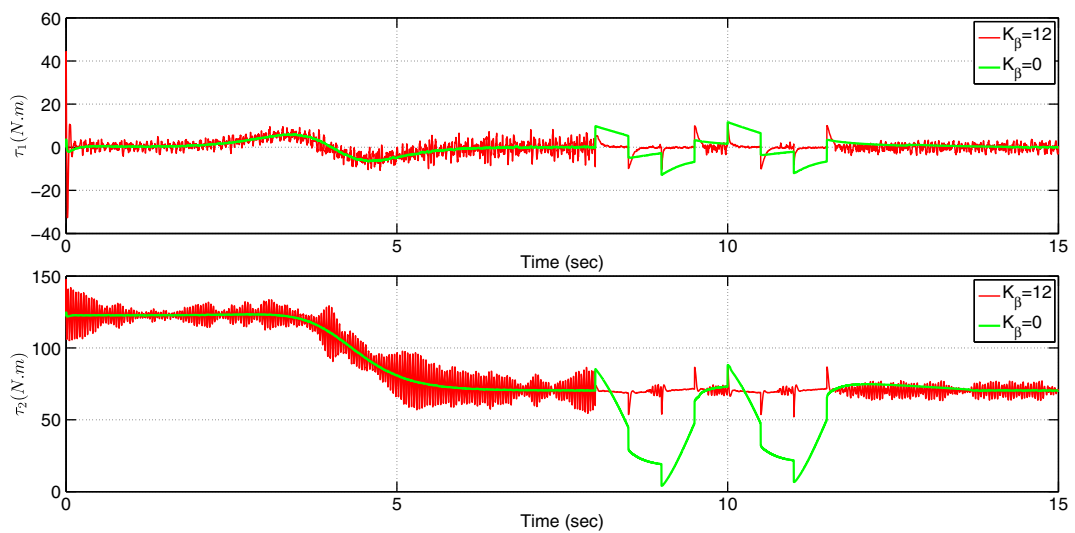
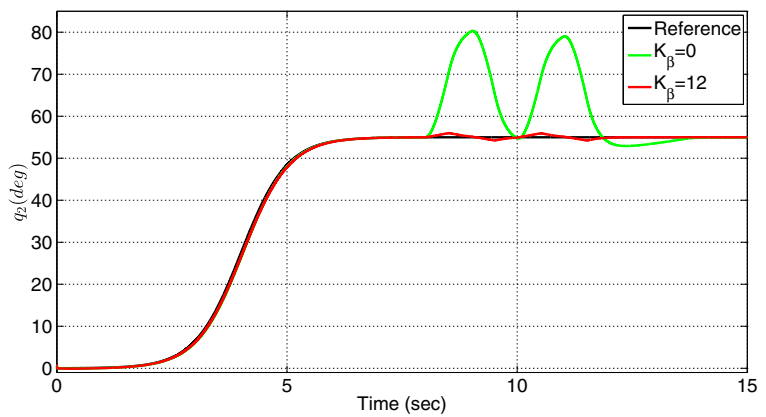


Fig. 22 Torque control inputs of the azimuth and elevation axes

Fig. 23 Estimated pitch angles

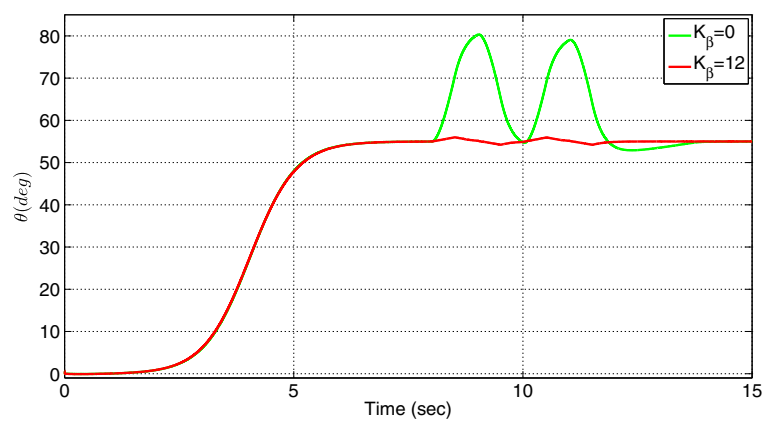


Fig. 24 Estimated yaw angles

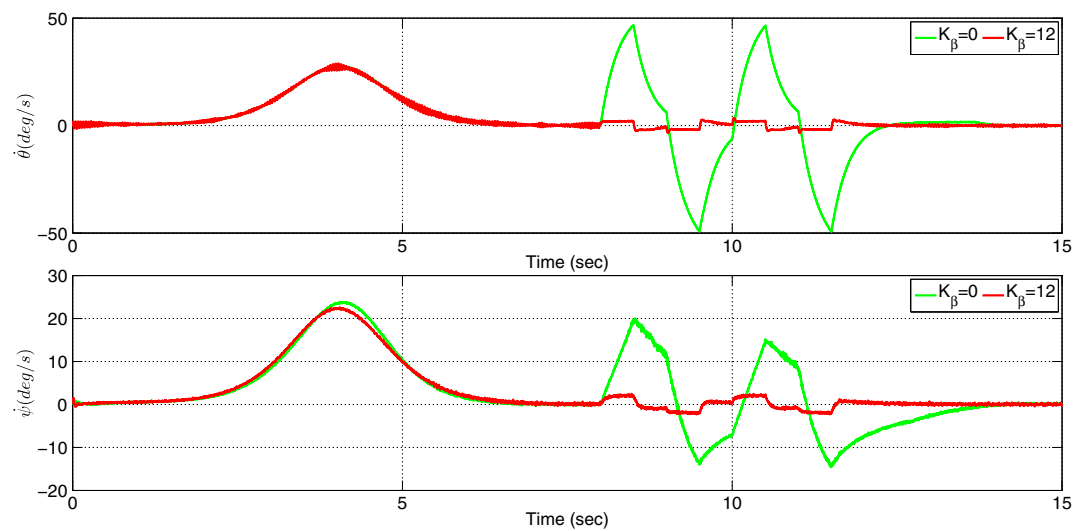
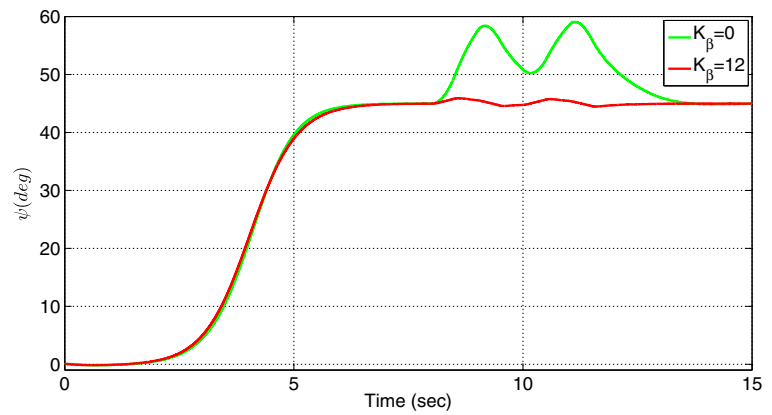


Fig. 25 Estimated Euler velocities

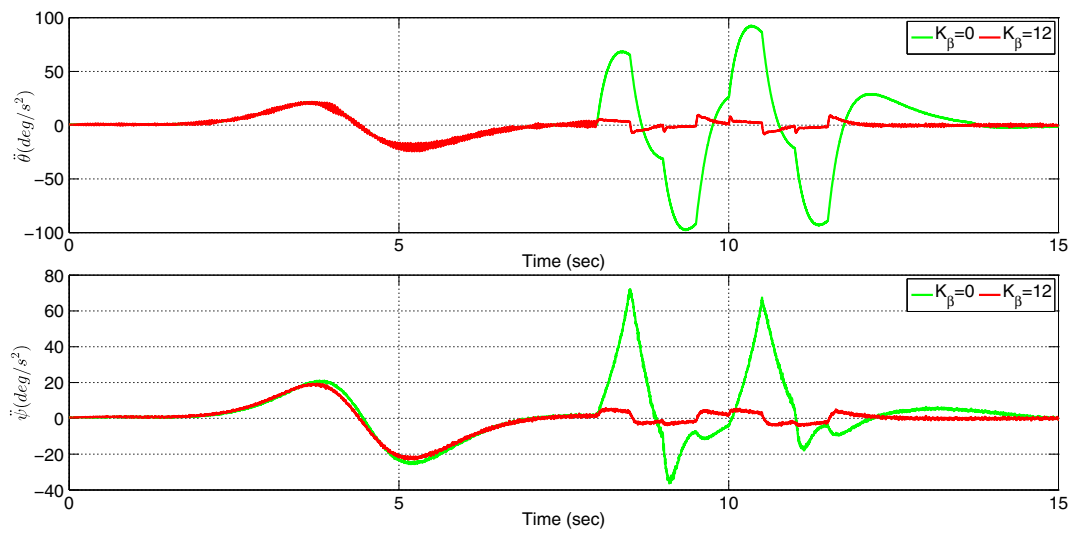


Fig. 26 Estimated Euler accelerations

Fig. 27 Estimated angular velocities about x axis

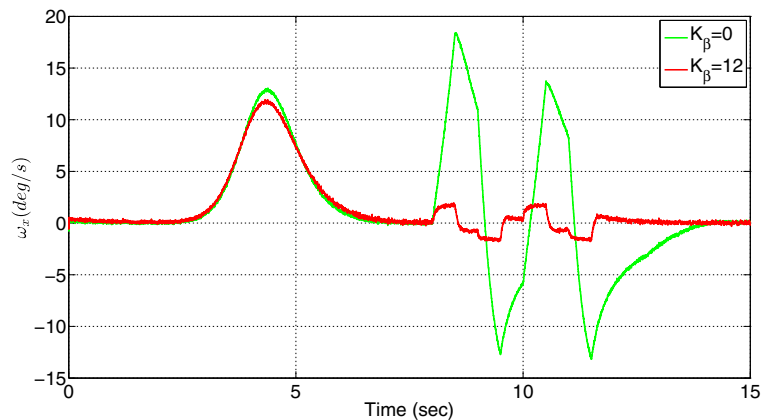


Fig. 28 Estimated angular velocities about y axis

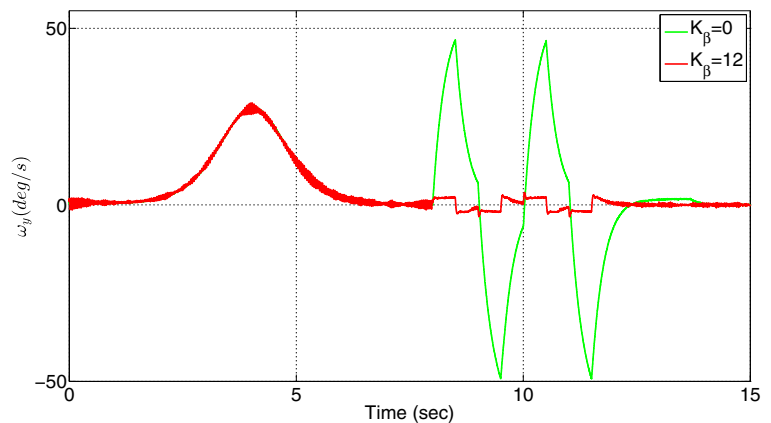


Fig. 29 Estimated angular velocities about z axis

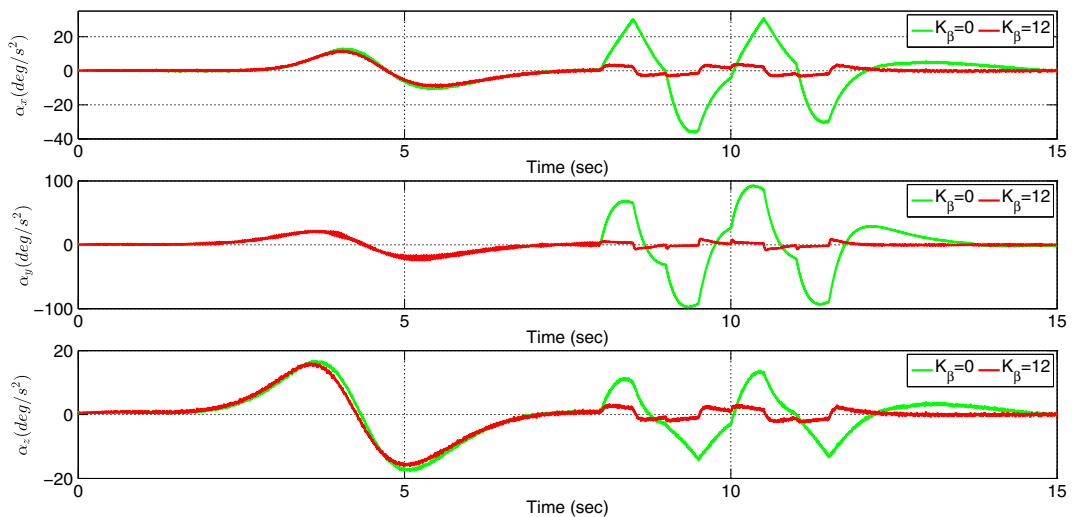
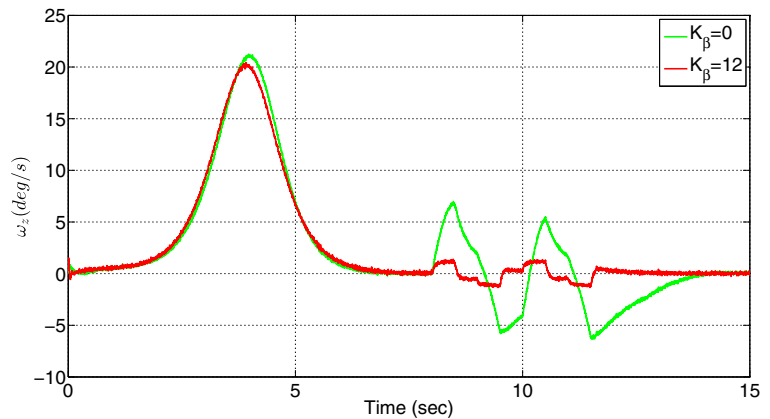


Fig. 30 Estimated angular accelerations

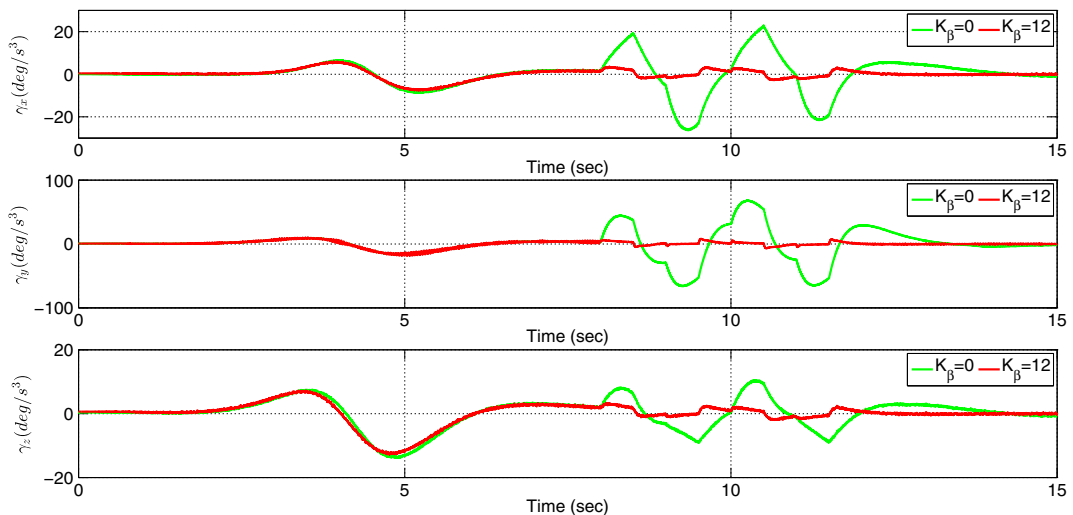


Fig. 31 Estimated angular jerks

Figures 27, 28 and 29 present the estimated angular velocities by the slave filter. When the acceleration feedback is not used, high amplitude angular velocities are obtained between $t = 8 \text{ sec}$ and $t = 12 \text{ sec}$ due to the sudden shocks. The dramatic changes are also observed in the estimated angular accelerations and jerks when the sudden shocks are applied on the system as depicted in Figs. 30 and 31.

5.2 Comparison with Other Sensor Fusion Algorithms

The performance of the proposed sensor fusion algorithm is compared to a Newton predictor enhanced Kalman filter (NPEKF) [25] and an error state Kalman filter (ErKF) [43, 44]. In the NPEKF method, angular accelerations are estimated by a classical Kalman filter and then estimated accelerations are passed through the Newton predictor to further reduce the phase lag caused by the Kalman filter. To compare the performance of the proposed method with NPEKF, pitch and yaw accelerations are estimated by the proposed filter and then those estimated values are passed through the following predictor designed by Han et.al [25]:

$$\mathbb{H}_2^1(z) = 3 - 3z^{-1} + z^{-2} \quad (34)$$

where $\mathbb{H}_2^1(z)$ represent 1-step 2nd-order Newton predictor. Thus, only three past states are required to predict pitch and yaw accelerations. To the best of our knowledge, the global Kalman filter and ErKF

have not been used to estimate Euler and body frame angular accelerations. However, there are attempts to solve the attitude estimation problem by using ErKF and underline differences between EKF and ErKF [43, 44]. Thus, advantages of ErKF over EKF are known for the attitude estimation. While ErKF is used to only estimate the errors in the state, EKF is implemented to obtain the state estimate itself. In this work, the performance of EKF that is used in a master-slave configuration with the inverse Φ -algorithm is compared with ErKF for the velocity and acceleration estimation problem. ErKF is also used in a master-slave configuration with the inverse Φ -algorithm since the process dynamics of this estimation problem requires to use body frame angular accelerations and jerks estimated by the inverse Φ -algorithm. The estimated signals by the proposed filter, NPEKF and ErKF are presented in Sections 5.2.1 and 5.2.2.

5.2.1 First Scenario

The performance of the proposed filter is compared to the Newton predictor and the error state Kalman filter while the system is exposed to random and continuous disturbances given in Fig. 6. Figures 32 and 33 present estimated pitch and yaw angles. The performance of the proposed filter is almost similar with the fusion algorithm where the master filter is designed as ErKF. However, estimated angles by NPEKF are noisy. Thus, the proposed method outperforms the Newton predictor.

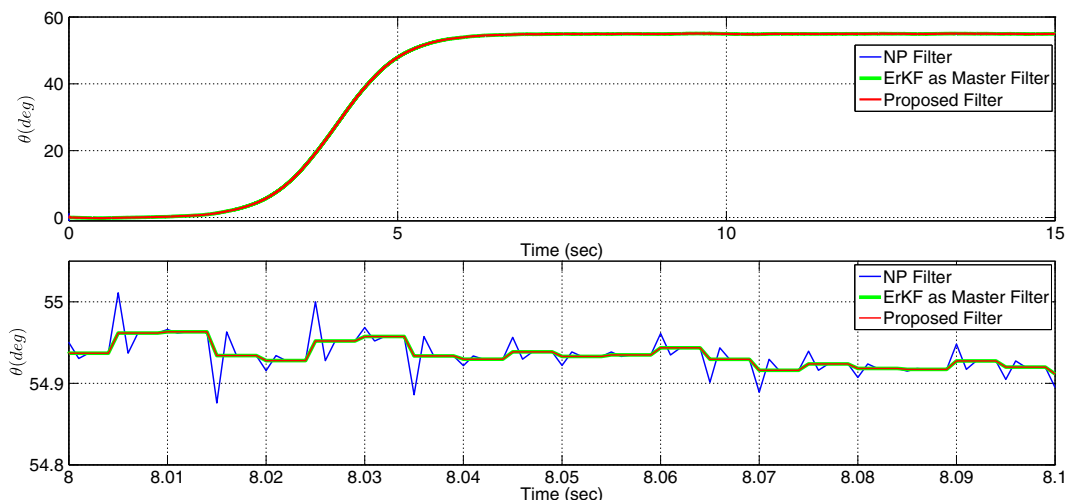


Fig. 32 Comparison between estimated pitch angles

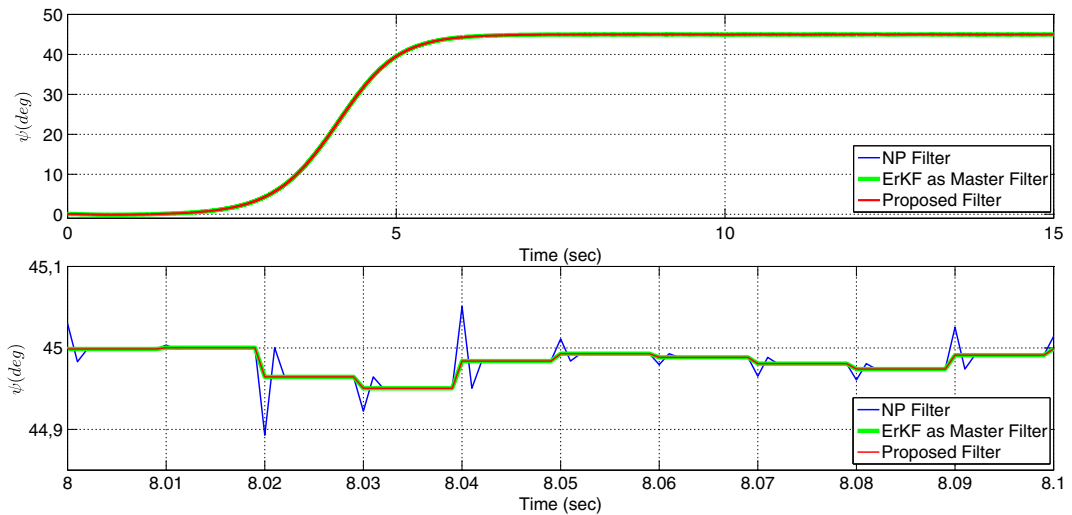


Fig. 33 Comparison between estimated yaw angles

Fig. 34 Error between measured and estimated pitch angles

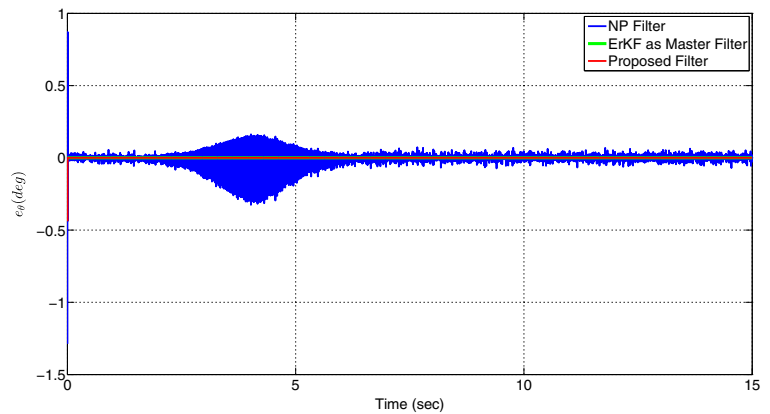
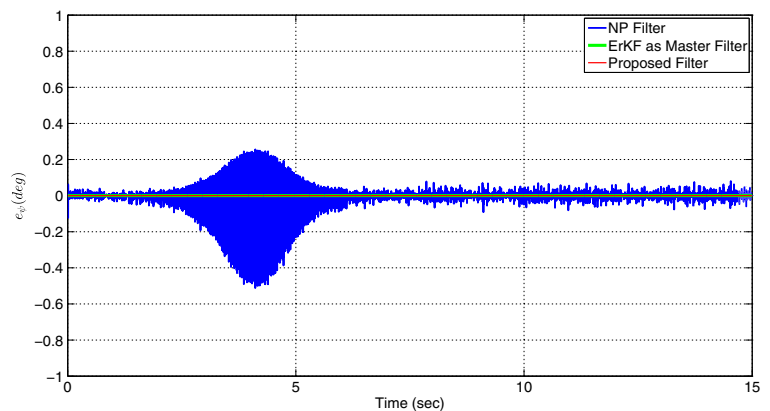


Fig. 35 Error between measured and estimated yaw angles



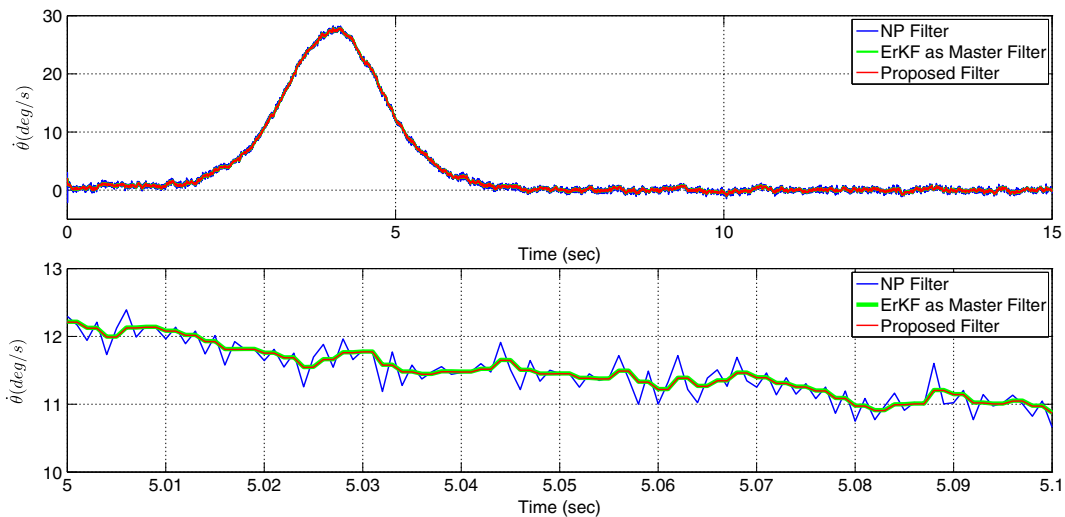


Fig. 36 Comparison between estimated pitch velocities

Errors between measured and estimated pitch and yaw angles are provided in Figs. 34 and 35. Estimation errors are almost the same when the master filter is implemented as either EKF or ErKF, but errors of NPEKF are larger than the ones obtained by the proposed filter. RMS values of the pitch angle estimation errors are 2.11×10^{-6} deg and 0.0451 deg for the proposed filter and NPEKF, respectively. RMS

value of the yaw angle estimation error is 0.0451 deg for NPEKF and smaller RMS error is obtained with the proposed method, i.e. 2.11×10^{-7} deg. Similar observations can be also done for the estimated values of pitch and yaw velocities and accelerations in Figs. 36, 37, 38 and 39. Estimated velocity and acceleration signals by the proposed method are closer to the ones estimated by the fusion algorithm in which

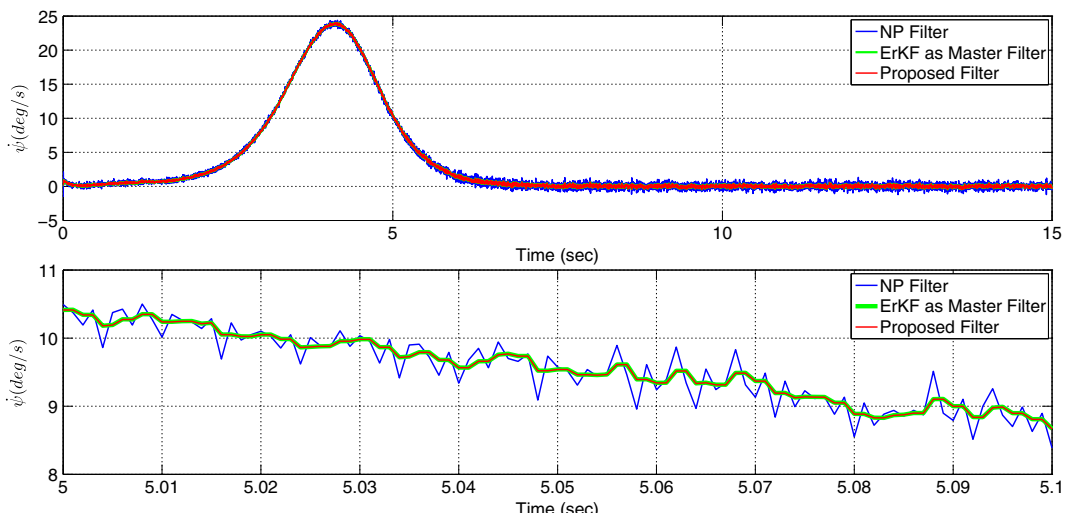


Fig. 37 Comparison between estimated yaw velocities

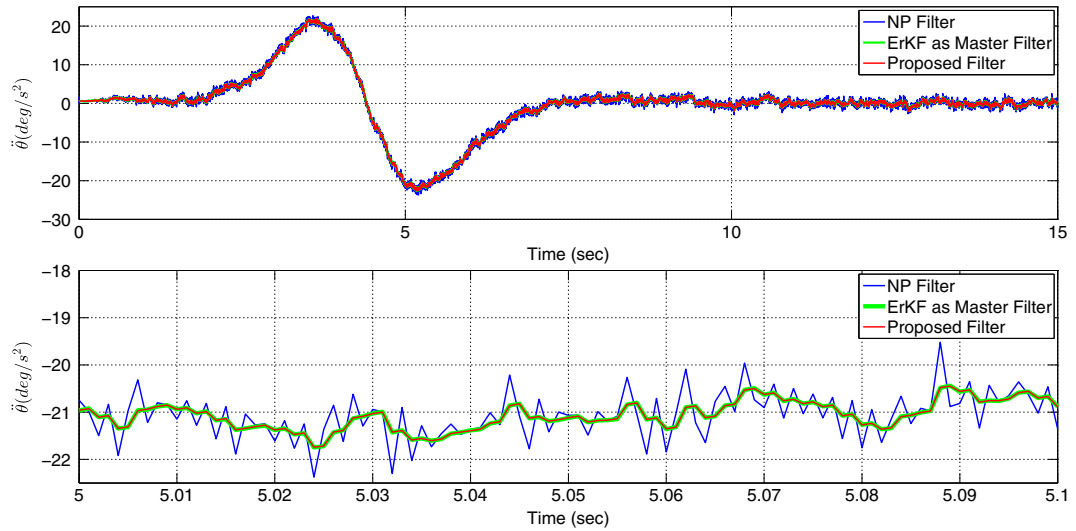


Fig. 38 Comparison between estimated pitch accelerations

the master estimator is implemented as ErKF. On the other hand, estimated signals are smoother with the proposed method compared to NPEKF.

5.2.2 Second Scenario

The performance of the proposed filter is compared to the Newton predictor and the error state Kalman filter when the sudden shocks are applied on the system. Estimated pitch and yaw angles are provided

in Figs. 40 and 41. Similar to the case of the first scenario, estimated pitch and yaw angles by the proposed method and the fusion algorithm in which the master filter is implemented as ErKF, are almost the same. On the other hand, better estimation performance is achieved with the proposed filter compared to NPEKF because the proposed one provides smoother estimates than NPEKF. Newton predictor leads to high amplitude peaks in estimated pitch and yaw angles.

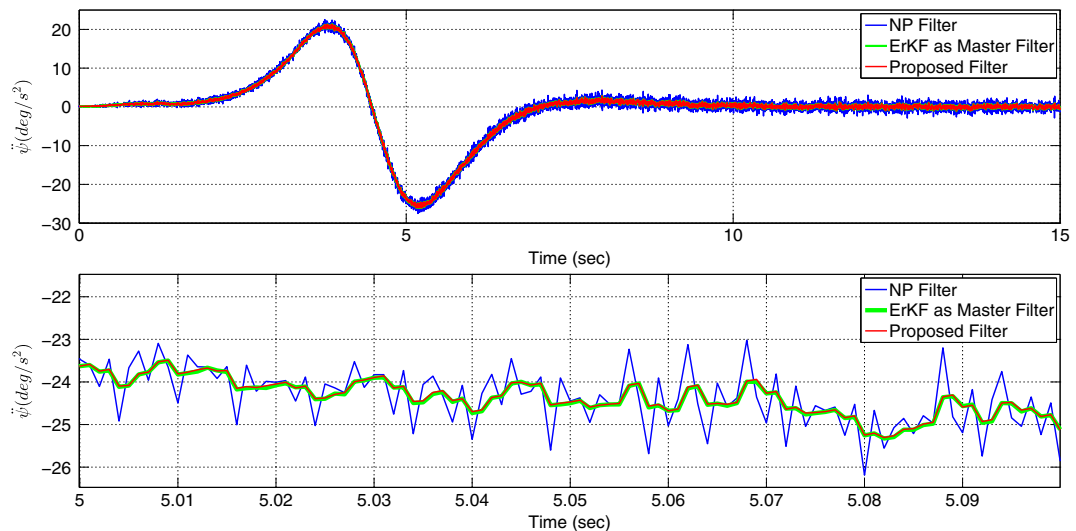


Fig. 39 Comparison between estimated yaw accelerations

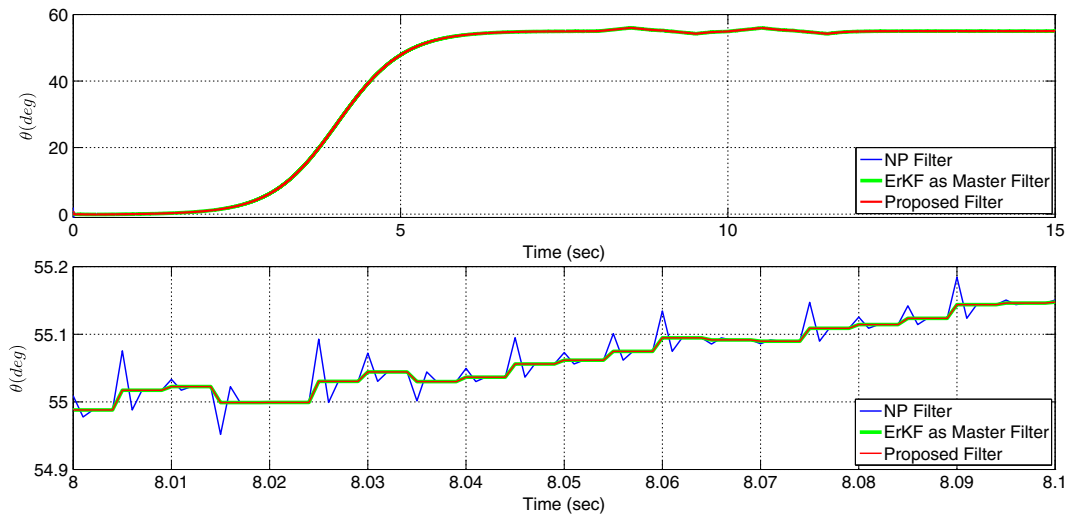


Fig. 40 Comparison between estimated pitch angles

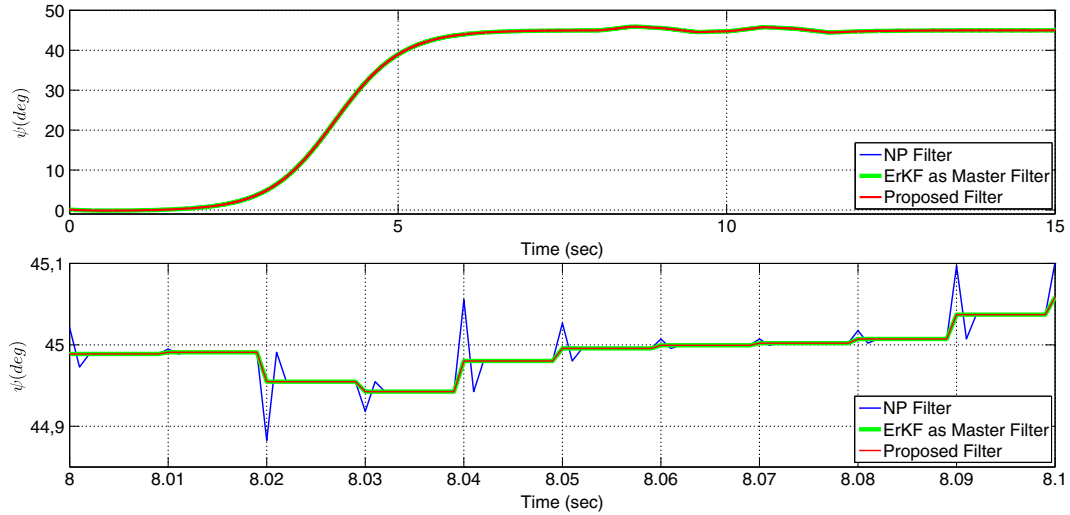


Fig. 41 Comparison between estimated yaw angles

Fig. 42 Error between measured and estimated pitch angles

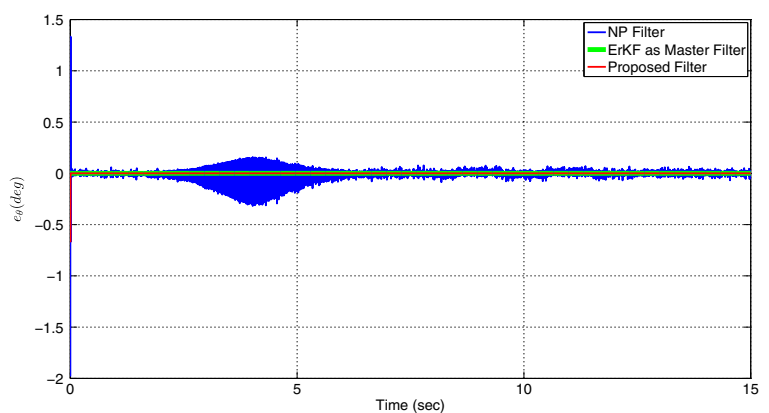


Fig. 43 Error between measured and estimated yaw angles

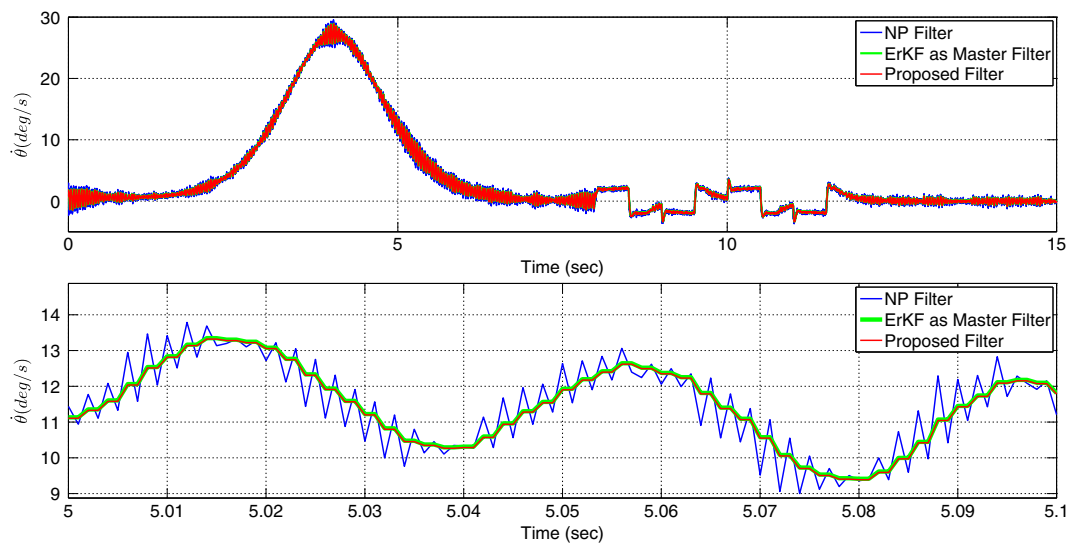
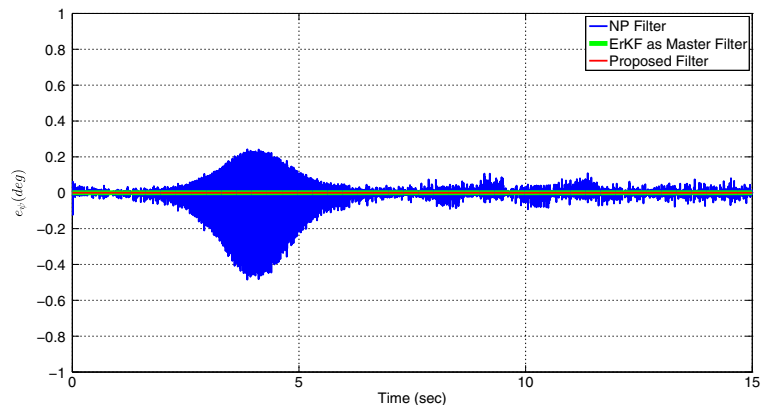


Fig. 44 Comparison between estimated pitch velocities

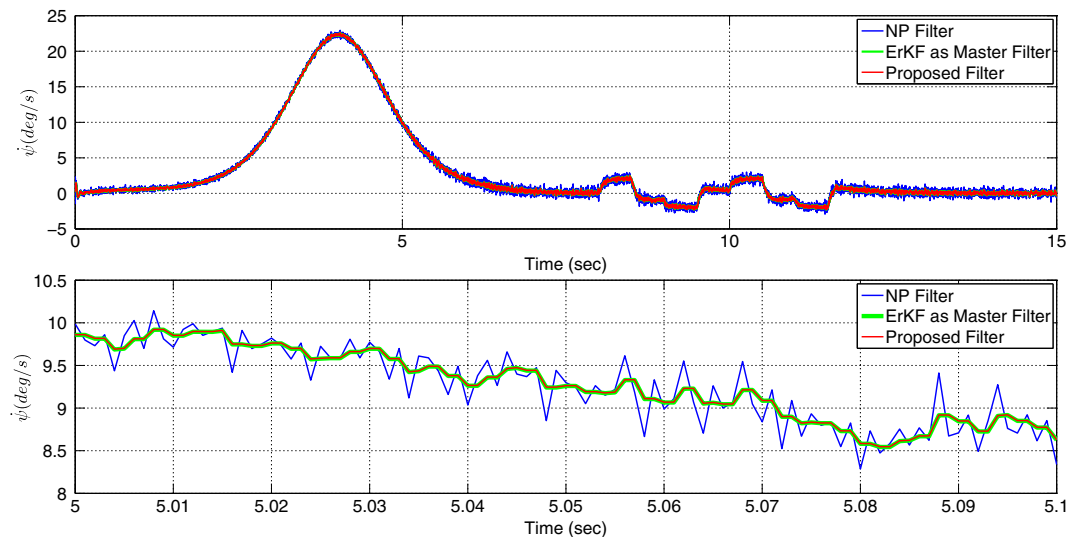


Fig. 45 Comparison between estimated yaw velocities

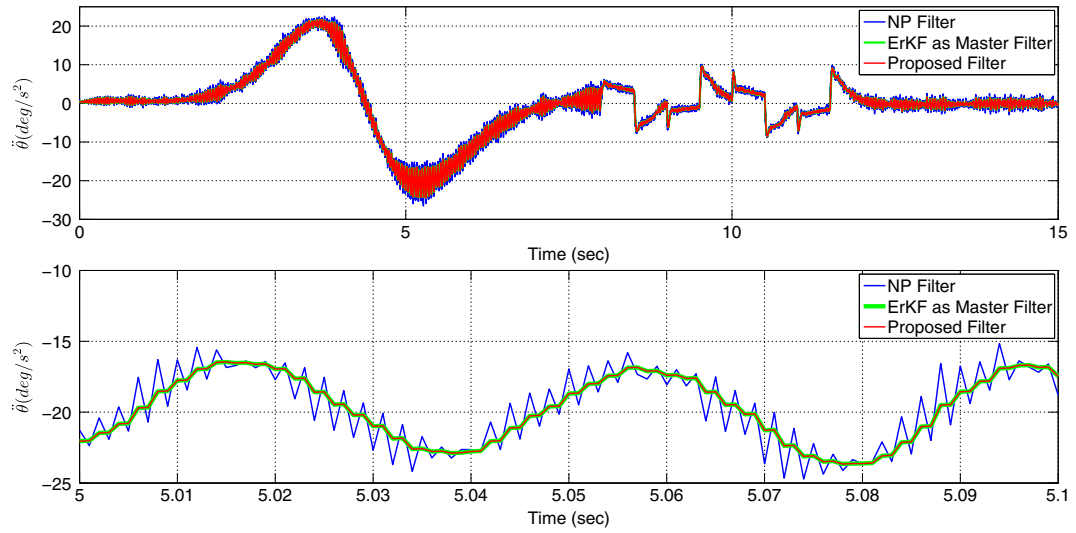


Fig. 46 Comparison between estimated pitch accelerations

Figures 42 and 43 also depict the errors between measured and estimated pitch and yaw angles. Estimation errors that are obtained by designing the master filter as either EKF or ErKF are similar. Those errors are also smaller than the ones computed with NPEKF. While RMS value of the pitch angle estimation error is 0.0481 deg for NPEKF, this RMS value decreases to $9.63 \times 10^{-6} \text{ deg}$ as the proposed method is utilized. On the other hand, RMS values of the yaw angle estimation errors are $2.05 \times 10^{-7} \text{ deg}$ and 0.0483 deg for the proposed filter and NPEKF, respectively.

Estimated pitch and yaw velocities and accelerations are also presented in Figs. 44, 45, 46 and 47. Similar velocities and accelerations are estimated by the proposed method and the fusion algorithm where the master estimator is implemented as ErKF. However, estimated signals by NPEKF have much more noise than the proposed filter. When the sudden shocks are applied on the system, oscillations occur in all estimated velocity and acceleration signals between $t = 8 \text{ sec}$ and $t = 12 \text{ sec}$, but the amplitudes of those oscillations are larger with NPEKF.

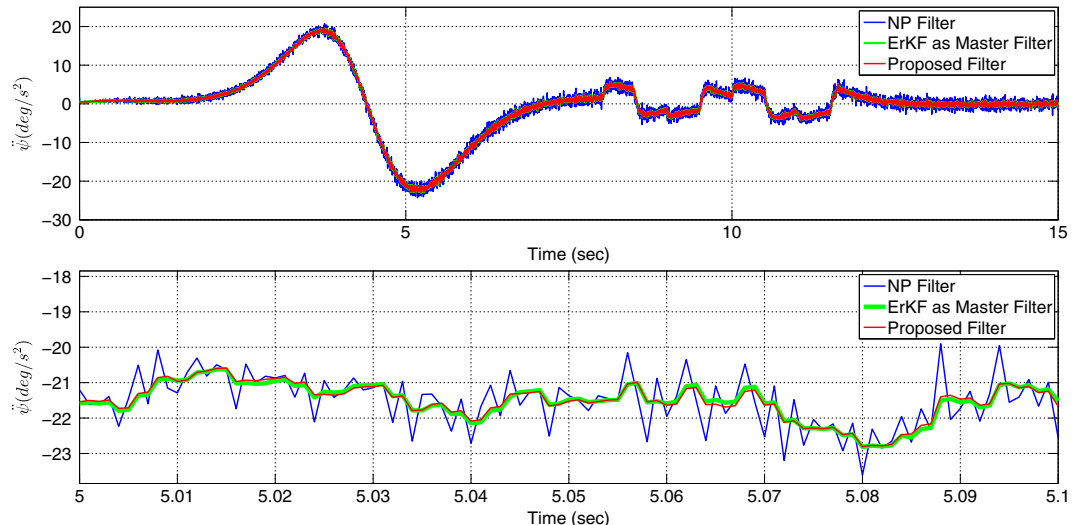


Fig. 47 Comparison between estimated yaw accelerations

6 Conclusion and Future Work

We have now presented a novel master-slave Kalman filter to estimate reliable Euler velocity and acceleration signals besides Euler angles. Slave estimator based on the inverse Φ -algorithm estimates angular velocities, accelerations and jerks. When these estimates are used in the master estimator, Euler angles, velocities and accelerations are estimated. The stabilization performance of the pan-tilt system is assessed by using estimated Euler angles, velocities and accelerations in a high fidelity simulation platform for two different disturbance scenarios. In the first scenario, the pan-tilt mechanism is subject to random and continuous time varying disturbances whereas sudden shocks in the form of short duration pulses with relatively large amplitudes are applied to the system in the second scenario. In the first scenario, azimuth angle converges in a smoother way by utilizing acceleration controller whereas small steady state errors are observed in the elevation angle response with the use of acceleration feedback. The amplitudes of the torque control inputs are almost the same with or without the use of acceleration feedback. Thus, acceleration control provides better performance without larger control efforts. Due to the sudden shocks in the second scenario, system responses have high amplitude oscillations when the acceleration controller is not active. As the acceleration feedback is introduced, the external disturbances are successfully rejected so much more smoother responses are achieved. Although high control efforts are obtained as the sudden shocks are applied on the system, the system has not been stabilized without the acceleration controller.

The performance of the proposed sensor fusion algorithm was compared to the Newton predictor enhanced Kalman filter (NPEKF) and the error state Kalman filter (ErKF) in both scenarios. Estimated angle, velocity and acceleration signals by the proposed master-slave Kalman filter and the fusion algorithm in which the master estimator is implemented as ErKF, are similar to each other. On the other hand, the proposed method outperforms NPEKF. The Newton predictor leads to much more noisy estimates and has the largest estimation errors compared with the other methods.

As a future work, various control algorithms such as adaptive control and robust control that utilize acceleration feedback will be developed and compared

with the performance of the controller used in this work. Furthermore, issues related to the bandwidth of the sensors used in the proposed sensor fusion algorithm will be fully explored. Experimental verification of the fusion algorithm and acceleration control on a physical system are also planned.

Appendix

The inverse Φ -algorithm assumes the following process and measurement models [35]:

$$x_k = A_{k-1}x_{k-1} + \Upsilon_{k-1}\epsilon_{k-1} \quad (35)$$

$$y_k = C_kx_k + \varepsilon_k \quad (36)$$

$$\varepsilon_k = \Psi_{k-1}\epsilon_{k-1} + \varsigma_{k-1} \quad (37)$$

$$\Psi_{k-1} = e^{-\frac{T}{\kappa}}, \quad R_k = \sigma^2(I - \Psi_{k-1}^2) \quad (38)$$

$$E(\epsilon_k) = E(\varsigma_k) = 0 \quad (39)$$

$$\begin{aligned} E(\epsilon_k \epsilon_l^T) &= Q_k \delta_{kl}, \quad E(\varsigma_k \varsigma_l^T) = R_k \delta_{kl}, \\ E(\epsilon_k \varsigma_l^T) &= 0 \end{aligned} \quad (40)$$

where A_{k-1} is the state transition matrix, C_k is the output matrix, ϵ_{k-1} and ς_{k-1} are the white Gaussian noises with zero means, ε_k is time correlated noise, $E(x)$ is the expectation of x , δ_{kl} is the Kronecker delta function, Q_k and R_k are the covariance matrices of ϵ_k and ς_k , Ψ_{k-1} is the transition matrix of the time correlated error, T is the sampling time, κ is the time constant, I is the identity matrix, and σ is the standard deviation.

Prediction stage of the inverse Φ -algorithm:

$$\hat{x}_{k/k-1} = A_{k-1}\hat{x}_{k-1/k-1} \quad (41)$$

$$P_{k/k-1} = A_{k-1}P_{k-1/k-1}A_{k-1}^T + Q_{k-1} \quad (42)$$

Update stage of the inverse Φ -algorithm:

$$\begin{aligned} K_k &= \left[P_{k/k-1} \bar{C}_k^T + S_k \right] \\ &\times \left[\bar{C}_k P_{k/k-1} \bar{C}_k^T + \bar{R}_k + \bar{C}_k S_k + S_k^T \bar{C}_k^T \right]^{-1} \end{aligned} \quad (43)$$

$$\hat{x}_{k/k} = \hat{x}_{k/k-1} + K_k [\bar{y}_k - \bar{C}_k \hat{x}_{k/k-1}] \quad (44)$$

$$\begin{aligned} P_{k/k} = & P_{k/k-1} - K_k \left[\bar{C}_k P_{k/k-1} \bar{C}_k^T + \bar{R}_k \right. \\ & \left. + \bar{C}_k S_k + S_k^T \bar{C}_k^T \right] K_k^T \end{aligned} \quad (45)$$

where

$$\bar{y}_k = y_k - \Psi_{k-1} y_{k-1} \quad (46)$$

$$\bar{C}_k = C_k - \Psi_{k-1} C_{k-1} A_{k-1}^{-1} \quad (47)$$

$$S_k = Q_{k-1} \Upsilon_{k-1}^T A_{k-1}^{-T} C_{k-1}^T \Psi_{k-1}^T \quad (48)$$

$$\bar{R}_k = \Psi_{k-1} C_{k-1} A_{k-1}^{-1} \Upsilon_{k-1} Q_{k-1} \Upsilon_{k-1}^T A_{k-1}^{-T} C_{k-1}^T \Psi_{k-1}^T + R_{k-1} \quad (49)$$

References

- Sukkarieh, S., Nebot, E.M., Durrant-Whyte, H.F.: A high integrity IMU/GPS navigation loop for autonomous land vehicle applications. *IEEE Trans. Robot. Autom.* **15**(3), 572–578 (1999)
- Wendel, J., Meister, O., Schlaile, C., Trommer, G.F.: An integrated GPS/MEMS IMU navigation system for an autonomous helicopter. *Aerospace Sci Technol.* **10**(6), 527–533 (2006)
- Jeong, S.H., Jung, S., Tomizuka, M.: Attitude control of a quad-rotor system using an acceleration-based disturbance observer: an empirical approach. *IEEE/ASME International Conference on Advanced Intelligent Mechatronics*. 916–921 (2012)
- Kalman, R.E.: A new approach to linear filtering and prediction problems. *J Basic Eng-T ASME* **82**(1), 35–45 (1960)
- Kim, A., Golnaraghi, M.F.: A quaternion-based orientation estimation algorithm using an inertial measurement unit. *IEEE Position Location and Navigation Symposium*. 268–272 (2004)
- Sabatini, A.M.: Kalman filter based orientation determination using inertial/magnetic sensors: Observability analysis and performance evaluation. *Sensors* **11**(10), 9182–9206 (2011)
- Mathieu, P., Denis, G.: Comparison between the unscented Kalman Filter and the extended Kalman filter for the position estimation module of an integrated navigation information system. *IEEE Intelligent Vehicles Symposium*. 831–835 (2004)
- Li, W., Wang, J.: Effective adaptive Kalman filter for MEMS-IMU/magnetometers integrated attitude and heading reference systems. *J. Navig.* **66**(1), 99–113 (2013)
- Roumeliotis, S.I., Sukhatme, G.S., Bekey, G.A.: Circumventing dynamic modeling: evaluation of the error-state Kalman filter applied to mobile robot localization. In: Proceedings of the 1999 IEEE International Conference on Robot Localization, pp. 1656–1663 (1999)
- Panich, S.: Indirect Kalman filter in mobile robot application. *J. Math. Stat.* **6**(3), 381–384 (2010)
- Mahony, R., Hamel, T., Pflimlin, J.M.: Nonlinear complementary filters on the special orthogonal group. *IEEE Trans. Autom. Control* **53**(5), 1203–1218 (2008)
- Bachmann, E.R., McGhee, R.B., Yun, X., Zyda, M.J.: Inertial and magnetic posture tracking for inserting humans into networked virtual environments. *Proc ACM Symp Virtual Real Softw Technol*. 9–16 (2001)
- Madgwick, S.O., Harrison, A.J., Vaidyanathan, R.: Estimation of IMU and MARG orientation using a gradient descent algorithm. *IEEE Int Conf Rehabil Robot*. 1–7 (2011)
- Gomes, M.S., Ferreira, A.M.: Gun-turret modelling and control. *ABCM Symposium Series in Mechatronics*. **2**, 60–67 (2005)
- Kumar, P., Dick, A., Sheng, T.S.: Real time target tracking with pan tilt zoom camera. *Digital Image Computing: Techniques and Applications*. 492–497 (2009)
- Davis, J., Chen, X.: Calibrating pan-tilt cameras in wide-area surveillance networks. *IEEE International Conference on Computer Vision*. 144–149 (2003)
- Lee, C.H., Kim, S.H., Kang, S.C., Kim, M.S., Kwak, Y.K.: Double-track mobile robot for hazardous environment applications. *Adv. Robot.* **17**(5), 447–459 (2003)
- Schmidt, P.B., Lorenz, R.D.: Design principles and implementation of acceleration feedback to improve performance of dc drives. *IEEE Trans. Ind. Appl.* **28**(3), 594–599 (1992)
- Deur, J., Peri, N.: A comparative study of servosystems with acceleration feedback. *IEEE Industry Applications Conference*. **3**, 1533–1540 (2000)
- Kobayashi, H., Katsura, S., Ohnishi, K.: An analysis of parameter variations of disturbance observer for haptic motion control. *IECON*. 1907–1912 (2005)
- Rubaai, A., Ofoli, A.R., Cobbina, D.: Dsp-based real-time implementation of a hybrid H_∞ adaptive fuzzy tracking controller for servo-motor drives. *IEEE Trans. Ind. Appl.* **43**(2), 476–484 (2007)
- Rezac, M., Hurac, Z.: Vibration rejection for inertially stabilized double gimbal platform using acceleration feed-forward. *IEEE International Conference on Control Applications*. 363–368 (2011)
- Craig, J.J., Hsu, P., Sastry, S.S.: Adaptive control of mechanical manipulators. *Int. J. Robot. Res.* **6**(2), 16–28 (1987)
- Xu, W., Han, J., Tso, S.: Experimental study of contact transition control incorporating joint acceleration feedback. *IEEE/ASME Trans. Mechatron.* **5**(3), 292–301 (2000)
- Han, J., He, Y., Xu, W.: Angular acceleration estimation and feedback control: an experimental investigation. *Mechatronics* **17**(9), 524–532 (2007)
- Chen, J.H., Lee, S.C., DeBra, D.B.: Gyroscope free strap-down inertial measurement unit by six linear accelerometers. *J. Guid. Control. Dyn.* **17**(2), 286–290 (1994)
- Edwan, E., Knedlik, S., Loffeld, O.: Constrained angular motion estimation in a gyro-free IMU. *IEEE Trans. Aerosp. Electron. Syst.* **47**(1), 596–610 (2011)
- Edwan, E., Knedlik, S., Loffeld, O.: Angular motion estimation using dynamic models in a gyro-free inertial measurement unit. *Sensors* **12**, 5310–5327 (2012)
- Petkov, P., Slavov, T.: Stochastic modeling of MEMS inertial sensors. *Cybern. Inf. Technol.* **10**(2), 31–40 (2010)

30. Crassidis, J.L., Markley, F.L., Cheng, Y.: Survey of non-linear attitude estimation methods. *J. Guid. Control. Dyn.* **30**(1), 12–28 (2007)
31. Lefferts, E.J., Markley, F.L., Shuster, M.D.: Kalman filtering for spacecraft attitude estimation. *J. Guid. Control. Dyn.* **5**(5), 417–429 (1982)
32. Diebel, J.: Representing attitude: Euler angles, unit quaternions, and rotation vectors. *Matrix* **58**(15–16), 1–35 (2006)
33. Shalom, Y.B., Li, X.R., Kirubarajan, T.: Estimation with applications to tracking and navigation, John Wiley and Sons (2001)
34. Collinson, R.P.G.: Introduction to avionics systems Springer (2003)
35. Wang, K., Yong Li, C.R.: Practical approaches to Kalman filtering with time-correlated measurement errors. *Trans. Aerosp. Electron. Syst.* **48**(2), 1669–1681 (2012)
36. Bryson, A.E., Henrikson, L.J.: Estimation using sampled data containing sequentially correlated noise. *J. Spacecr. Rocket.* **5**(6), 662–665 (1968)
37. Petovello, M.G., O’Keefe, K., Lachapelle, G.: Consideration of time-correlated errors in a Kalman filter applicable to GNSS. *J. Geod.* **83**(1), 51–56 (2009)
38. Petovello, M.G., O’Keefe, K., Lachapelle, G., Cannon, M.E.: Erratum to: Consideration of time-correlated errors in a Kalman filter applicable to GNSS. *J. Geod.* **85**, 367–368 (2011)
39. Tao, G., Ma, X.: Backlash compensation for multivariable nonlinear systems with actuator dynamics, IEEE Decis Contr. 3382–3387 (1999)
40. Hori, Y.: Disturbance suppression on an acceleration control type DC servo system. *IEEE Power Electron.* 222–229 (1988)
41. Tian, F., Craig, K., Nagurka, M.: Disturbance attenuation in a magnetic levitation system with acceleration feedback. *IEEE International Conference on Industrial Technology.* 59–64 (2011)
42. Craig, K.: Acceleration feedback
43. Setoodeh, P., Khayatian, A., Farjah, E.: Attitude estimation by separate-bias Kalman filter-based data fusion. *JNAV* **57**, 261–273 (2004)
44. Madyastha, V.K., Ravindra, V.C., Mallikarjunan, S., Goyal, A.: Extended Kalman Filter vs. Error State Kalman Filter for Aircraft Attitude Estimation. *Guidance, Navigation and Control Conference* (2011)

Sanem Evren received her B. S. Degree in Systems Engineering from Yeditepe University, Istanbul, Turkey in 2005 and M.S. degree in Mechatronics Engineering from Sabanci University, Istanbul, Turkey in 2012. Since then, she has been a research assistant and Ph.D. candidate in the Faculty of Engineering and Natural Sciences, Sabanci University. Her research interests include control theory, robotics, sensor fusion, visual servoing, coordinated motion of multiple robots, development of wind energy systems.

Firat Yavuz received his B.S. degree in Mechatronics Engineering from Bahcesehir University, Istanbul, Turkey in 2014. Since then, he has been a research assistant and M.S. candidate in the Faculty of Engineering and Natural Sciences, Sabanci University. His research interests are control systems, sensor fusion and robotics.

Mustafa Unel received the B.S. degree in Electrical and Electronic Engineering and the M.S. degree in Systems and Control Engineering from Bogazici University, Istanbul, Turkey in 1994 and 1996, respectively. He received a second M.S. degree in Applied Mathematics and the Ph.D. degree in Electrical Sciences and Computer Engineering from Brown University, RI, USA in 1998 and 1999, respectively. During 1999–01, he was a postdoctoral fellow at Brown and Yale Universities. In Spring 2001, he joined the Department of Computer Engineering at Gebze Institute of Technology, Turkey as an assistant professor. Since Fall 2004, he has been with the Faculty of Engineering and Natural Sciences, Sabanci University, Istanbul, Turkey. Dr. Unel became an Associate Professor in 2005 and a Full Professor in 2011. Dr. Unel’s research interests are in computational vision, control, visual servoing, unmanned aerial vehicles, robotics and microsystems. He has published more than 90 technical papers in these areas. He is on the editorial board of the International Journal of Mechatronics and Manufacturing Systems.